

EFFECT OF WIDTHWISE WEB THICKNESS  
NONUNIFORMITIES ON WOUND ROLL  
STRESSES

By

ENG SHENG NGOI

Bachelor of Science

Oklahoma State University

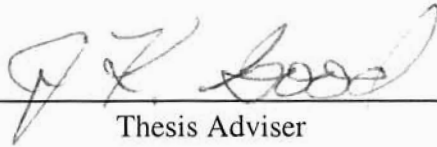
Stillwater, Oklahoma

1999

Submitted to the Faculty of the  
Graduate College of the  
Oklahoma State University  
in partial fulfillment of  
the requirements for  
the Degree of  
MASTER OF SCIENCE  
December, 2002

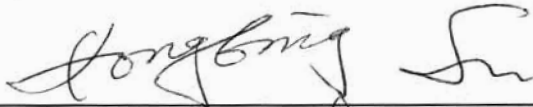
EFFECT OF WIDTHWISE WEB THICKNESS  
NONUNIFORMITIES ON WOUND ROLL  
STRESSES

Thesis Approved:



---

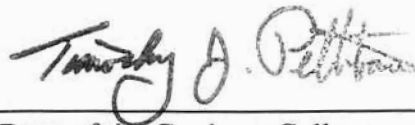
Thesis Adviser



---



---



---

Dean of the Graduate College

## **ACKNOWLEDGEMENT**

I am deeply indebted to my advisor Dr. J. K. Good for his stimulating suggestions and encouragement that helped me in all the time of research and writing of this thesis. He is a great person to work with.

Mr. Ron Markum deserves a special mention here, without whose assistance our work in the WHRC would have been impossible. I would like to thank Dr. H. Lu and Dr. C.E. Price for their acceptance to be in my committee. I would also like to thank other research associates in the WHRC who have made it a great working environment.

Finally, I would thank my parents for their love and support throughout this whole process.

## TABLE OF CONTENTS

Chapter	Page
<b>1. INTRODUCTION</b>	<b>1</b>
<b>2. LITERATURE SURVEY</b>	<b>3</b>
2.1 Experimental Methods For Studying Wound Roll Structure	3
2.2 3D Wound Roll Models	6
2.3 Current Modeling Efforts At The WHRC	7
<b>3. EXPERIMENTAL SETUP</b>	<b>11</b>
3.1 Selection of Roll Structure Measurement Methods For Rolls Wound From Non-Uniform Thickness Webs	11
3.2 Design of a Winder Core	12
3.3 Winding Machine Description and Winding Conditions	19
3.4 Material Testing	23
3.4.1 Thickness Profile of Webs Across the Web Width	24
3.4.2 In-Plane Modulus ( $E_t$ ) Test	25
3.4.3 Friction Tests	26
3.4.4 Radial Modulus Tests	27
<b>4. EXPERIMENTAL RESULTS AND DISCUSSION</b>	<b>30</b>
4.1 In-roll Pressure Dependency on Web Widthwise Thickness and Nip Load	30
<b>5. CONCLUSIONS</b>	<b>40</b>
<b>FUTURE WORK</b>	<b>41</b>
<b>REFERENCES</b>	<b>42</b>
<b>APPENDIX A</b>	<b>44</b>



## LIST OF TABLES

Table	Page
Table 3.1 Experimental Results of Strain Gages CMD under Diametral Loading.....	17
Table 3.2. Results of In-Plane Modulus Tests for Various Web Materials.....	25
Table 3.3. Coefficient of Friction Factors.....	27
Table 3.4 Coefficients of K1 and K2 in Pfeiffer's Equation.....	29
Table 4.1 Surface Roughness of 3Mil PET Web.....	36
Table A-1 Numerical Core Pressure Data for 3mil PET Web.....	48
Table A-2 Numerical Core Pressure Data for 2mil PET Web.....	51

## LIST OF FIGURES

Figures	Page
Figure 3.1 Winder Core with Strain Gages Attached.....	15
Figure 3.2 Winder-Nip Roll Retracted.....	16
Figure 3.3 Winder in Operation-Nip Roll Engaged.....	16
Figure 3.4 Experimental set up.....	20
Figure 3.5 Web Line User Interface.....	21
Figure 3.6 Web Line Tension Signals of HSWL.....	23
Figure 3.7. Widthwise Thickness Profile of 2-Mil and 3-Mil PET Webs.....	25
Figure 3.8. Stress-strain Curve for 3-mil PET for In-plane Modulus Test.....	26
Figure 3.9 Radial Moduli of PET Webs.....	29
Figure 4.1. Repeatability Tests for Center Wound Rolls With 3.33 pli of Nip Load and 1 pli Web Tension.....	31
Figure 4.2. Core Pressure Profile For the 2-Mil PET Web Wound at a Web Tension of 1 pli .....	32
Figure 4.3. Core Pressure Profile For the 2-Mil PET Web Wound at a Web Tension of 1 pli and Nip Load of 3.33 pli.....	32
Figure 4.4. Core Pressure Profile For the 2-Mil PET Web Wound at a Web Tension of 1 pli and Nip Load of 3.33 pli.....	34
Figure 4.5. Core Pressure Profile For the 2-Mil PET Web Wound at a Web Tension of 1 pli and Nip Load of 6.67 pli.....	34
Figure 4.6. Core Pressure Profile For the 3-Mil PET Web Wound at a Web Tension of 1 pli.....	35

Figure 4.7. Core Pressure Profile For the 3-Mil PET Web Wound at a Web Tension of 2 pli.....	36
Figure 4.8. Core Pressure Profile For the 3-Mil PET Web Wound at a Web Tension of 1 pli and Nip Load of 3.33 pli.....	38
Figure 4.9. Core Pressure Profile For the 3-Mil PET Web Wound at a Web Tension of 1 pli and Nip Load of 6.67 pli.....	38
Figure 4.10. Core Pressure Profile For the 3-Mil PET Web Wound at a Web Tension of 2 pli and Nip Load of 3.33 pli.....	39
Figure 4.11. Core Pressure Profile For the 3-Mil PET Web Wound at a Web Tension of 1.5 pli and Nip Load of 6.67 pli.....	39
Figure A-1: Web Guide of HSWL.....	45
Figure A-2: Rewind Station of HSWL.....	45
Figure A-3: Nip Station 1 of HSWL.....	46
Figure A-4: Nip Station 2 of HSWL.....	46
Figure A-5: Unwind Station of HSWL.....	47
Figure A-6: Stress-strain Curve for 2-mil PET for In-plane Modulus Test.....	47

## NOMENCLATURE

$T_w$	Winding Tension
$\mu$	Coefficient of Friction
$\mu_k$	Kinetic Coefficient of Friction
$\mu_{A/w}$	Aluminum to Web Kinetic Coefficient of Friction
$\mu_{w/w}$	Web to Web Kinetic Coefficient of Friction
K1	Preiffer's Coefficient- A material constant and it is the value of pressure on the sheets when the strain is reduced to zero(psi)
K2	Springness Factor, Dimensionless
WOT	Wound-on-Tension(pli)
$E_t$	In-plane Modulus (psi)
$E_r$	Radial Modulus (psi)
h	Web Thickness (in)
$\epsilon$	Strain (in/in)
$\sigma_r$	Radial Stress (psi)
$\sigma_\theta$	Circumferential Stress (psi)
a	Core Inside Radius (in)
b	Core Outside Radius (in)
V	Web Velocity (in/s)

$\theta$	Wrap Angle (rad)
$S_y$	Yield Stress (psi)
$S_g$	Gage Factor
$R_a$	Average Surface Roughness (micro-in)
$R_q$	Root Mean Square Surface Roughness (micro-in)
$\eta$	Dynamic Viscosity of Air (lb. s/ ft)

# CHAPTER 1

## INTRODUCTION

Several products are produced in the form of a web. The webs are wound on a core to provide internal stability and so they can be shipped to other manufacturers. These manufacturers will unwind and rewind the web through different processes. There are several winder configurations used in winding webs, such as center winding, center winding with a nip roller and surface winding. Web materials include textiles, rubbers, steel, paper, nonwovens, film/foil laminates, countertops, wallpapers, and carpets. The length dimension of these materials far exceeds the width dimension, and the width dimension far exceeds the thickness.

In center winding with an impinging nip roller, the driving torque is applied to the core while the nip roller is undriven. Today the majority of winders apply a nip to the wound roll. In this winding method, radial pressure is applied by the nip roller to the wound roll at the point where the web enters the roll. This reduces the air entrainment into the roll and increases the tension of the web entering the roll. In surface winding, the torque is supplied to the nip roller and the core is undriven.

The quality of a wound roll is dependent on the stresses that exist on it. Winding rarely improves the quality of a web but it is the only practical form for storing large amounts of web material. The in-roll stresses can damage the web. If the wound roll does not meet the quality requirements of the down stream user, it either has to be re-wound or scrapped. If there are many “bad” rolls, it can cause a substantial loss in profits.

An ideal web has uniform thickness in both the length and the width directions. Real webs, however, produced on extrusion drawing machines have thickness variations in both the width and the length directions. The width direction thickness variations in such webs can be persistent in the lengthwise direction. When webs with lengthwise-persistent widthwise thickness variations are wound, the resulting rolls tend to have hard streaks in the thick regions, which are areas of increased roll radius and increased interlayer pressure.

The objective of this research is to develop an experimental method for assessing pressure variation in rolls wound with webs which have variation in web thickness across the cross machine direction (CMD).

## CHAPTER 2

### LITERATURE SURVEY

The quality of a wound roll is highly dependent upon the in-roll stress distribution which is controlled by winder operating parameters such as center torque, nip load, web tension and others depending on the winder type. Damage can be caused to a web if in-roll stresses are not properly controlled. Pfeiffer [1] is one of the researchers to discuss this qualitatively. He observed that the rolls wound with an impinging nip roller produced a harder rolls as compared to those wound rolls without any nip.

#### **2.1 Experimental Methods for Studying Wound Roll Structure:**

Monk and Lautner [2] were the first to use pull tabs to measure the compressive pressure in the radial direction. The nylon tabs were inserted within a roll while the slitter was running, with one tab placed at the core and one for each inch of the roll thickness. The force required to move the tabs in the rolls was determined on an Instron tensile tester. The compressive pressures exerted on the tab by the roll were determined with a known coefficient of friction and the pull tab force.

Good, and Fikes [3], for the first time used Force Sensitive Resistors(FSRs) to measure the interlayer pressures in a wound roll. They presented a technique by which the FSRs could be calibrated for experimental studies of the radial pressure profile in wound rolls. The results of such wound roll studies have led to the discovery of a new



boundary condition that allows stress models, previously constrained to center winding, to be applied to center winding with an undriven nip roll pressed against the wound roll . The FSRs not only can be used to measure interlayer pressures at various radii in the wound roll, but them can also used to measure the pressure variations across the width of the web in the CMD.

Rand and Eriksson [4] analyzed the stresses in newsprint rolls theoretically and experimentally in center winding. They established the stress state in the roll both in completed rolls and during the winding process. Strain gages were attached onto the web, which provided continuous information about stresses in the web during the entire winding process. Strain was obtained as the web passed onto the winding roll and under the nip roller in their studies. The signals were fed through slip rings from the roll to a chart recorder for registration. They stated that the radial stress in the roll must be great enough to prevent slippage on the core during winding and that the radial stress was constant throughout the roll for their web and winder operating parameters.

Hakiel [5] center wound a resin-coated paper on aluminum cores at various tensions. Immediately after winding, the rolls were evaluated using a “punch test” to determine inter-layer pressure by forcibly causing them to telescope at several different diameters. The evaluation was performed on a mechanical testing machine using machined dies to force the wound roll to slip laterally at the radius of the dies. The interlayer pressure was simply determined by dividing the experimentally measured

telescoping force by the area of a lap at the appropriate diameter and by the coefficient of friction of the web against itself.

Hakiel's and Cole's [6] used a segmented-instrumented core to measure interlayer pressures due to widthwise thickness variations of the webs. The core consisting of twelve independent segments and each segment was instrumented with two strain gages which measured the circumferential contraction of the segment. All of the segments were mounted on a common inner core by means of rubber "O-rings" and were pinned to the inner core with three pins. This allowed the segments to contract radially and independently of each other and of the inner core. The interlayer pressures and in-roll stresses were determined with an algorithm described in [5] once the widthwise distribution of tension is determined for all of the laps in the wound roll.

Kedl's [7] model also predicted the pressure and circumferential stress in a center winding roll due to thickness variations over the web width. He compared pressures predicted by his model to pressures measured using FSRs. Twenty nine FSRs on one inch spacing were silk screened on a common backing. These transducers were wound into rolls at various radii such that pressure could be monitored across the roll width and as a function of radius. Kedl also made some use of the pull tab method which has been used previously to measure pressures in narrow rolls. Traditionally the pull tab extends out on both sides of the wound roll. Thus, when the pull force is measured, which is the force required to dislodge the tab, the area of contact does not change. Kedl used pull tabs of various lengths at a given radial location but spaced circumferentially about the roll. By

comparing the pull forces of the tabs of various lengths. He was able to discern how the pressure varied across the width of the roll.

Balaji [8] employed pull tabs to measure the pressure at several radial location in a wound roll. He developed a calibration curve for pressure versus force for each pull tab. The pull tabs were inserted into the wound roll in a direction perpendicular to the motion of the web. Once the roll is wound completely, the pull tabs are pulled thrice. The average value from the three pulls is used with the calibration curve to determine the radial pressure. The radial pressure determined is an average value over the width of the roll. Theoretically the pull force can be described as:

$$P = \int_A \mu \sigma_r dA \quad \text{Equation (2.1)}$$

where  $\mu$  is coefficient of friction between the tab and web materials

$\sigma_r$  is radial pressure

A is the contact area between the tab and the wound roll

## 2.2 3D Wound Roll Models:

Hakiel and Cole's [6] and Kedl's [7] models are two models which predict widthwise variability in wound roll radius and stresses resulting from widthwise thickness nonuniformities. Hakiel and Cole's model used an LVDT sensor to predict the roll profile across the width of the roll. Both models predict the widthwise variations in outside roll radius, winding tension, interlayer pressure and in-roll tension in a roll wound of a web with lengthwise-persistent widthwise thickness variations. These models treated

the roll as independent widthwise segments and computed the average winding tension for each of those segments and only looked at center winding. Both models portray the 3D roll as a series of 2D sectors, and that each sector is evaluated using a 2D winding model.

Both models require input in order to compute the wound roll stresses. The required inputs are core diameter, roll diameter, web thickness as a function of CMD location, Poisson's ratio, winding tension profile, core modulus, Young's modulus and stack modulus of the webs. The predicted wound roll stresses were later compared to measured wound roll stresses.

Kedl's model considered coupled in-roll displacements with the outer lap but neglected the dependence of stack modulus on load when calculating in-roll displacements. Hakiel and Cole presentation is similar to Kedl, in that coupling between the outer lap analysis and the in-roll displacements is accounted for. The major difference is that the coupling occurs at each lap while the roll is winding. This provides the means to retain the effect of the load-dependent stack modulus on in-roll displacements.

### **2.3 Current Modeling Efforts at the Web Handling Research Center(WHRC)**

Hoffecker at WHRC introduced a model code which is an axisymmetric finite element model (FEM). Hoffecker's model continuously represents the wound roll in the CMD without compatibility violations unlike the Kedl and Hakiel and Cole models . One of the limitations of these models is that the order in which the web thickness could be

rearranged and result in the same radial pressure profiles. So if the web thickness from the 1<sup>st</sup> sector is transferred to the fourth sector the pressure profile which was associated with the 1<sup>st</sup> sector will move to the fourth sector. This points to the independence of these sectors which may not represent reality. A second shortcoming of these models is the inability to predict stresses in a CMD direction which could be responsible for corrugations about the circumference of the wound roll. The FEM uses four-node quadrilateral web elements on the r-z plane and rotates about the z-axis to form a cylindrical web shell. In the core each web element is assigned a stiffness which interacts with other elements to produce winding stresses. Besides treating a continuous wound roll, the model will apply to the addition a nip roller with finite bending stiffness as well. In this model different CMD locations in the roll grow at different rates because of cross web thickness non-uniformities and variations in the applied nip load.

Good et al [9] presented a model to calculate the internal stresses within a wound roll which has been center wound with an undriven nip roller impinged upon the outside of the roll. In this model, Hakiel's wound roll model was modified to incorporate an undriven nip and the analytical results were backed up by experimental observations. They formulated a new boundary condition for wound roll stress models as given in Equation 2.2 in which the tension in the outer wrap was set equal to the sum of the incoming web stress and saturated value of nip induced tension. The mechanism was discovered as an elongating machine direction strain caused by compressive Hertzian-like contact stresses which exist beneath the nip roll location on the lower side web which is in intimate contact with the wound roll. A new boundary condition was presented for

winding models in terms of the coefficient of friction and nip loading in addition to web tension and web thickness.

$$\sigma_r|_{r=s} = \left[ \{T_w|_{r=s}\} + \frac{\mu N}{h} \right] \frac{h}{s} \quad \text{Equation (2.2)}$$

where N is Nip Loading

$\mu$  is kinetic coefficient of friction, web to web

h is web thickness

s is radial location of outer wrap

$T_w$  is web line tension

Balaji [8] performed a friction test to determine the coefficient of friction between the web and the aluminum roller and also between web layers. Balaji found that the coefficient of friction between a HDPE web and a Tyvek web(0.07) was much less than the kinetic friction coefficient(0.20).

Good, Hartwig and Markum [10] proposed a measurement of wound-on-tension(WOT) for center wound rolls with an undriven nip roll. They gave an equation for WOT,

$$WOT = T_w + \mu N \quad \text{Equation (2.3)}$$

where  $T_w$  is web tension (pli)

N is nip load (pli)

$\mu$  is friction coefficient between web layers

Thus with  $\mu$  being a fraction only a fractional component of the nip load becomes WOT.

Several methods discussed in the survey of literature were employed during this investigation into the wound roll stresses measurement method. The use of strain gages on a continuous core will be demonstrated later in this study.

3D winding models are a subject of on going research at Oklahoma State University. Models are being developed which eliminate the modeling of a 3D roll as a series of 2D rolls as Kedl [7] and Hakiel and Cole [6] assumed. Also the effect of an impinging nip on 3D roll is being studied.

The objective of this research is to develop an experimental means for studying stresses in 3D wound rolls which have been wound with an impinging nip roller. The results from these tests will show for the first time how web tension and nip-induced tension are apportioned to various widthwise locations depending on web thickness non-uniformity. These research results will be used to verify 3D models currently under development at OSU.

## CHAPTER 3

### EXPERIMENTAL SET-UP

#### 3.1 Selection of Roll Structure Measurement Methods For Rolls Wound From Non-Uniform Thickness Webs

Hakiel [5] punch test gave an average discrepancy of about 10% between theoretical and experimental results. The disadvantage of this method is that it cannot be used to measure the inter-layer pressure across the width of the web. It can only be used to measure the inter-layer pressure for narrow rolls but not for the inter-layer pressure CMD location of the web.

Kedl [7] used FSRs and pull tabs for measuring pressure spatially throughout the roll. There are difficulties in using FSR devices as their output resistance varies not only as a function of pressure but also with time and temperature, even at constant pressure. The advantage of pull tabs is that for narrow rolls they provide good pressure accuracy at multiple radial locations. The accuracy in using pull tabs of various lengths to discern pressures as a function of CMD location is less. The disadvantages of pull-tabs are that they are intrusive and are time and labor intensive. In addition, the pressure inferred must be interpreted as an integrated average pressure level across the roll width at that radial location.

After reviewing all of the advantages and disadvantages of the roll structure measurement methods, the core pressure method was chosen for this research experiment because of the relation between core pressure, and radial and circumferential strains and



stresses. Through proper design of wall thickness, diameter, and material selection, more than one microstrain circumferentially can be obtained for each psi of hydrostatic pressure.

### 3.2 Design of a Winder Core

An aluminum alloy (Al 6061-T6) was chosen to be the winder core for this research and it has a yield strength,  $S_y$ , of 39900 psi . Equations 3.1 and 3.2 show both the radial stress,  $\sigma_r$ , and tangential stress,  $\sigma_\theta$ , of a cylindrical shell with the internal pressure is zero by Shigley[11].

$$\sigma_\theta = \frac{-Pb^2}{b^2 - a^2} \left( 1 + \frac{a^2}{r^2} \right) \quad \text{Equation (3.1)}$$

$$\sigma_r = \frac{-Pb^2}{b^2 - a^2} \left( 1 - \frac{a^2}{r^2} \right) \quad \text{Equation (3.2)}$$

where b is the outer radius (in)

a is the inner radius (in)

P is the uniform external pressure (psi)

On the inner surface, a, the radial stress equals to zero and the maximum stress for an external pressure is in the tangential direction. With an outer and inner radii of 4.25-in and 3.95-in, respectively, the tangential stress is computed to be  $-14.68P$ . The maximum pressure which the aluminum core can withstand prior to a plastic failure is shown in Equation 3.3. The maximum external pressure prior to a plastic failure was found to be 2717 psi .

$$P_{\max} = \frac{S_y}{14.68} \quad \text{Equation (3.3)}$$

The aluminum winder core was also analyzed to determine if buckling of the core would occur. The magnitude of the critical pressure of buckling of a cylindrical shell under the action of uniform external lateral pressure is predicted by the equation given below by Timoshenko [12]. The result obtained from Equation 3.4 represents the correct values of the critical pressure only as long as the calculated compressive stresses are within the elastic region. Beyond the proportional limit Equation 3.4 gives exaggerated values for the critical pressure and to obtain satisfactory results the reduced modulus  $E_r$ , instead of  $E$ , should be used.

$$\frac{(1-\nu^2) q_{cr} a}{Eh} = \frac{1-\nu^2}{\left(n^2-1\right)\left(1+\frac{n^2 l^2}{\pi^2 a^2}\right)^2} + \frac{h^2}{12a^2} \left( n^2 - 1 + \frac{2n^2 - 1 - \nu}{1 + \frac{n^2 l^2}{\pi^2 a^2}} \right)$$

Equation(3.4)

- where
- $q_{cr}$  is the critical pressure (psi)
  - $E$  is the Young's modulus of the core (psi)
  - $h$  is the thickness of the core (in)
  - $a$  is the inter radius of the core (in)
  - $\nu$  is the Poisson's ratio
  - $n$  is the wave number  $\neq 1$
  - $l$  is the length of the core (in)

To obtain the lowest critical pressure, the wave number , $n$ , was chosen to be 2. With all the known values, the critical pressure was found to be 1155 psi.

The aluminum core was manufactured with a center-less grinding method for the high speed web line after the theoretical analysis was completed. This manufacturing method was chosen for the core to ensure concentricity between the inner diameter and outer diameter down the entire core length. Nine full strain gage bridges with 2.5-inch apart from each other were applied on the inner core surface to monitor core pressure across the roll width (36-inch) as rolls are wound on center winding and center wind with a nip. From the center of the core, which is 0 CMD location, full strain gage bridges were attached 2.5-inch apart to the right (positive sign) and left (negative sign) until they reached at 10-inch and -10-inch CMD locations. Figure 3.1 shows a view of winder core with strain gages attached. Two-element rosette strain gages were installed diametrically opposed to compose a full strain gage bridge. A Measurements Group model 3800 wide range strain indicator was used to monitor the strain changes due to pressure. Since the core is continuous, the pressure occurs at each location can affect the output of the neighboring bridges. The winder equipment is shown in figure 3.2 and figure 3.3 shows a roll wound at fixed constant nip load and web tension.

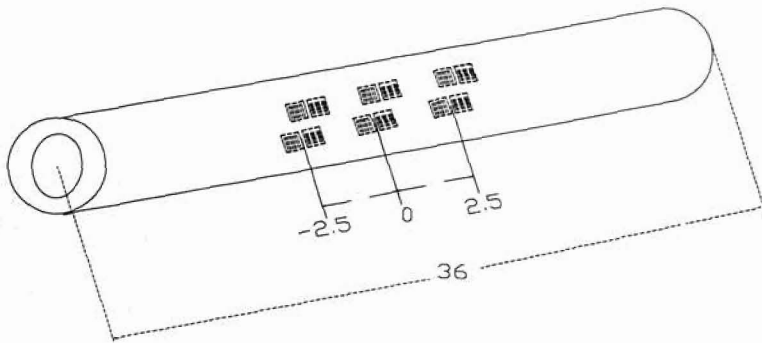


Figure 3.1 Winder Core with Strain Gages Attached CMD Locations.

With the instrumented core completed, a static test was devised to ensure all the strain gage bridges were performing properly. The core was placed in diametral compression in an Instron model 8500 servo hydraulic test system. The load was applied at the locations of the full bridges. Strain Indicator 3800 from Vishay Measurements Group was used to measure the strain outputs. The load was increased in 50lb increments and the strains were recorded as shown in Table 3.1. From the data it appears all channels are working with comparable outputs at a given load. Also the output of each channel appears to be varying linearly with respect to the diametral load. Thus, it appears all gages are bonded well to the inner wall of the core and that the connection of the Wheatstone bridges is adequate.

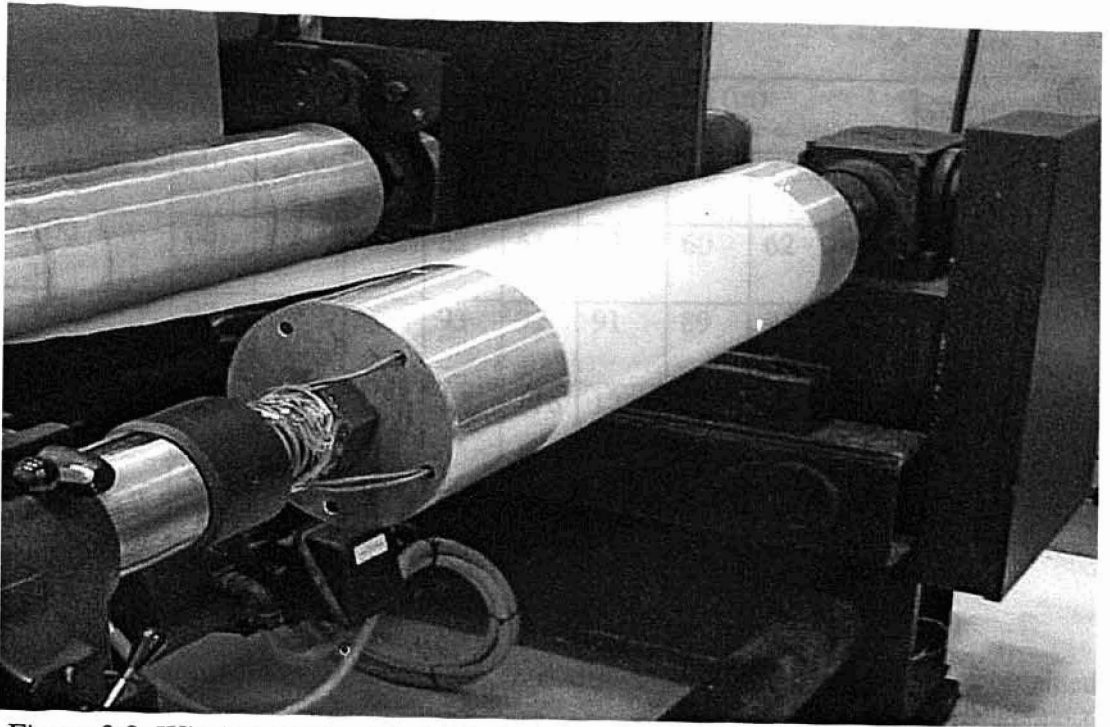


Figure 3.2. Winder- Nip Roll Retracted

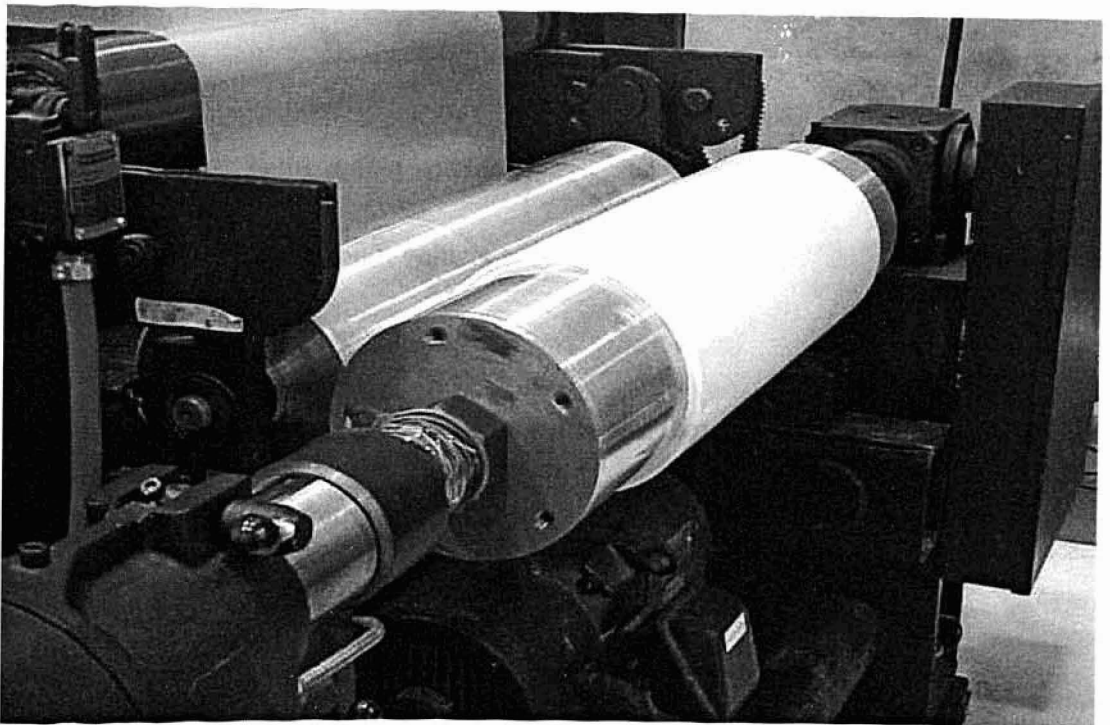


Figure 3.3. Winder in Operation- Nip Roll Engaged

Diametric Load (lb)	Experimental Strains CMD Location (in)								
	-10	-7.5	-5.0	-2.5	0	2.5	5.0	7.5	10.0
100	66	62	67	62	61	63	60	62	60
150	97	89	96	93	92	91	89	94	87
200	125	118	121	120	116	122	119	125	119
250	153	145	148	150	144	147	149	157	149

Table 3.1 Experimental Results of Strain Gages CMD Under Diametral Loading

Equation 3.5 aids in the proper interpretation of the strain results obtained from the standard four-arm bridge in addition to assisting the stress analyst in the proper placement and orientation of gages for experimental measurements.

$$\frac{e_o}{e_i} = \frac{S_g}{4} (\varepsilon_1 - \varepsilon_2 - \varepsilon_3 + \varepsilon_4) \quad \text{Equation (3.5)}$$

where  $e_o$  is the output voltage

$e_i$  is the input voltage

$S_g$  is the gage factor

$\varepsilon_1 - \varepsilon_4$  are all four strain gages and they depend on the orientation

From the orientation of strain gages inside the inner surface of the core,  $\varepsilon_1 = \varepsilon_4$  and

$\varepsilon_2 = \varepsilon_3$ . But  $\varepsilon_2 = -\nu\varepsilon_1$  and this yields

$$\frac{e_o}{e_i} = \frac{S_g (2(1+\nu))}{4} \varepsilon \quad \text{Equation (3.6)}$$

where  $\nu$  is the Poisson's ratio of the core (0.33)

With a Poisson's ratio of 0.33 in this case, a bridge factor of 2.66 is obtained from Equation 3.6. This means that every measured output from the model 3800 strain indicator for hydrostatic pressure will be multiplied by a ratio of 4/2.66 (1.5037) to obtain an actual strain output.

The core pressure can be obtained as shown in equation 3.7 by Dally [13] with known circumferential strain.

$$P_o = \frac{E\varepsilon_\theta(b^2 - a^2)}{2b^2(1 - \nu^2)} \quad \text{Equation (3.7)}$$

where  $P_o$  is the core pressure (psi)

$E$  is the Young's modulus of the core (psi)

$\varepsilon_\theta$  is the circumferential strain (in/in)

$\nu$  is the Poisson's ratio of the core

$b$  is the outer radius of the core (in)

$a$  is the inner radius of the core (in)

### 3.3 Winding Machine Description and Winding Conditions:

Figure 3.4 shows a diagram of the high speed web line. In this setup, the web is unwound from the unwinding station. The unwind is driven by a 35 Hp AC vector drive. Web tension is measured using an idler roll on load cells and this signal is used as a feedback signal to the drive control system to maintain constant tension. The web is then passed through a FIFE Model OPG-LRA web displacement guide which employs an infrared edge and a FIFE A-9 Signal Processor. The sensors and the guides play an important role in this setup by controlling the lateral position of the web. The web then passes through a series of driven rollers, web line tension load cell or dancer rolls depending on the mode of control in that tension zone.

As the web approaches the winding station it passes through a second FIFE web guide and web tension is measured. The web will then proceed directly to the winding core developed for this experiment if pure center winding is required. If center winding with an impinging nip roller is required the web proceeds around  $180^{\circ}$  around the nip roller onto the winding roll. The nip roller, 8 inches in diameter in this case, is mounted on a swing arm which is pushed into the winding roller with pneumatic rolling diaphragm force actuators. The swing arm is mounted upon a driven sled whose purpose is to maintain the swing arm in vertical attitude. This is done such that web tension will not affect nip load and thus web tension and nip load can be independently controlled. The winder drive is another Reliance 35 HP AC vector drive.



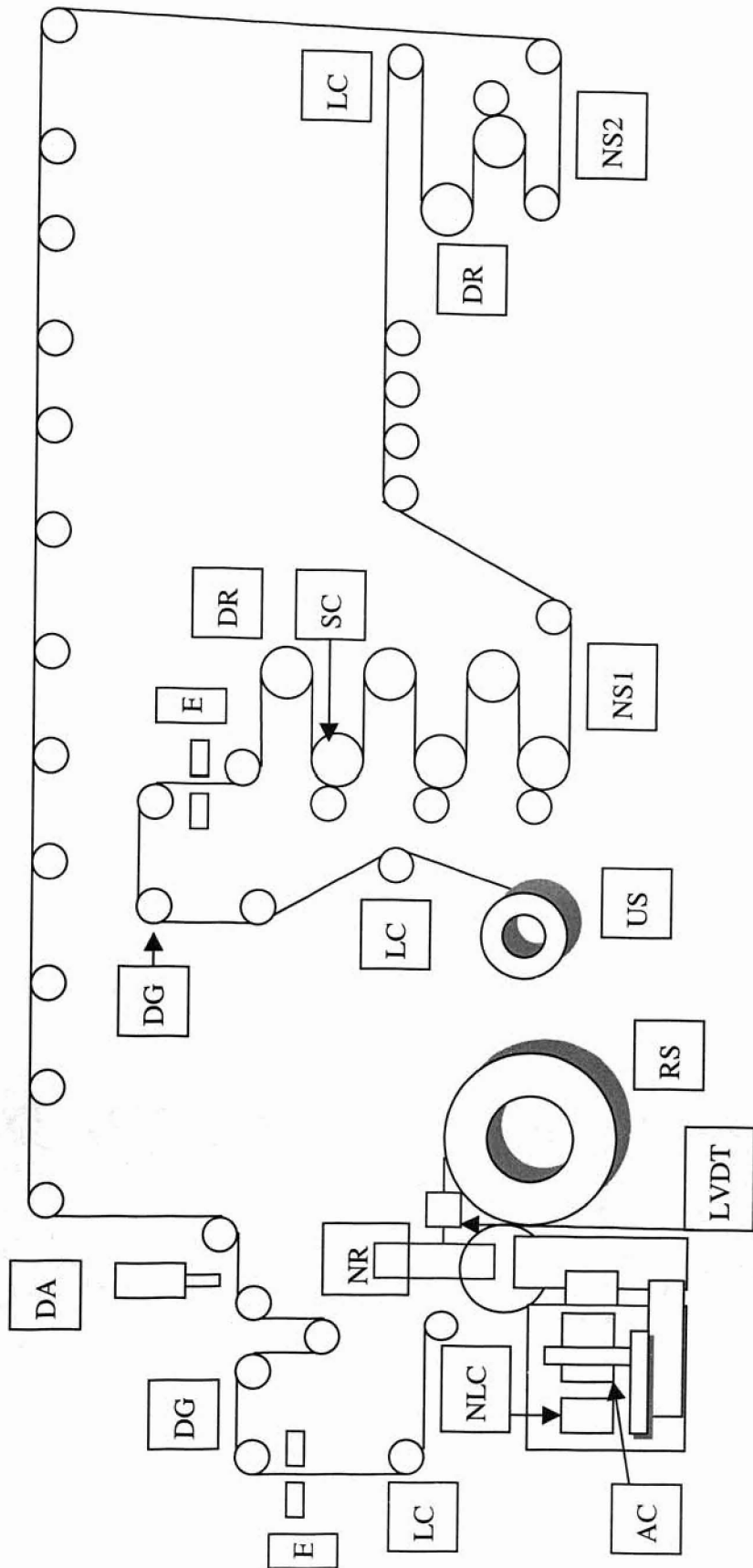


Figure 3.4 Experimental set up

AC: Air cylinder to apply nip load	NLC: Load cell to measure nip load
DA: Dancer actuator	NR: Nip roller
DG: Displacement guide	NS1: Nip station #1
DR: Dancer roller	NS2: Nip station #2
E: Edge sensor	RW: Rewind station
LC: Load cell	SC: Speed comparator
LVDT: Detects if swing arm is vertical	US: Unwind station

Figure 3.5 shows the web line user interface where all parameters and properties such as web line tension, speed, width and thickness of web, nip load, core diameter and winding methods (center winding, center winding with undriven nip roller, surface winding) are selected.

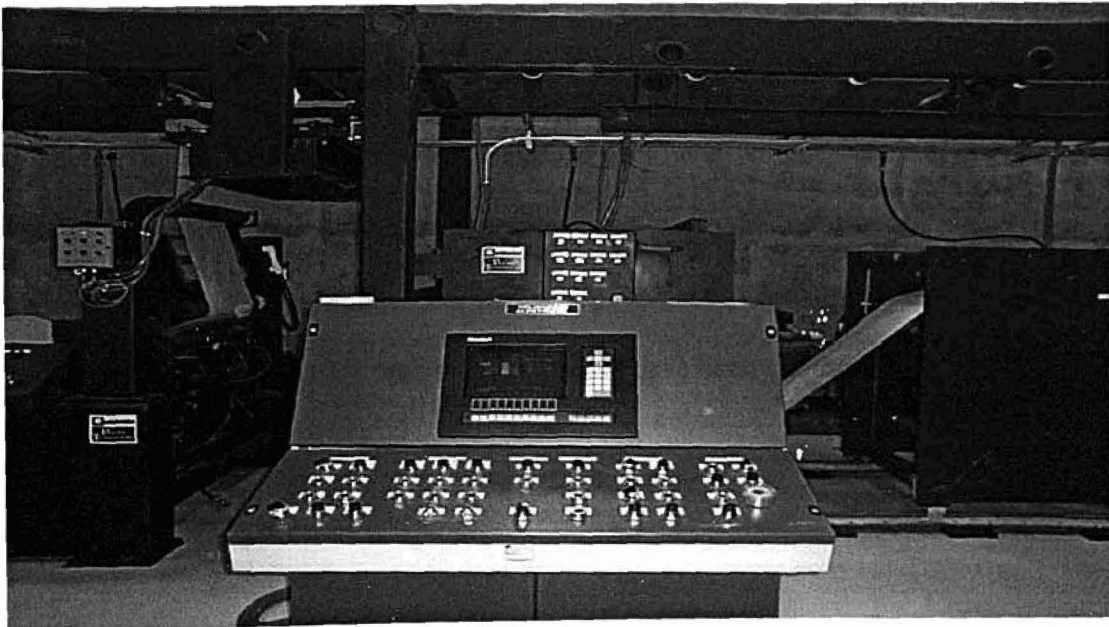


Figure 3.5. Web Line User Interface

Pagilla P.R. and Shelton J.J. [14] determined the performance of High Speed Web Line (HSWL) in terms of tension and speed regulation. A 20.5-inch wide Tyvek web was run at a web tension of 0.6 pli. Experimental data at various points on the HSWL for dancer feedback and load cell feedback with current feedback control strategies (PI) was collected. The data was later analyzed to determine tension and speed behavior. Figure 3.6 shows the experimental result of the web line tension signal of HSWL. It can be seen that the accuracy of web line tension is within  $\pm 3$  lbs. This accuracy is dependent upon the web line, the drive controls, and the web being handle.

The un\_load cell and NR3 load cell web tension signals shown in Figure 3.6 are made immediately downstream of the unwind station. Web tension in web lines typically has the largest dynamic components in the vicinity of the unwind stand. Unwinding rolls are typically non-concentric and the source of these dynamic components. Fortunately the winder is two tension zones downstream from the NR3 load cell such that these dynamic tension components have been attenuated.

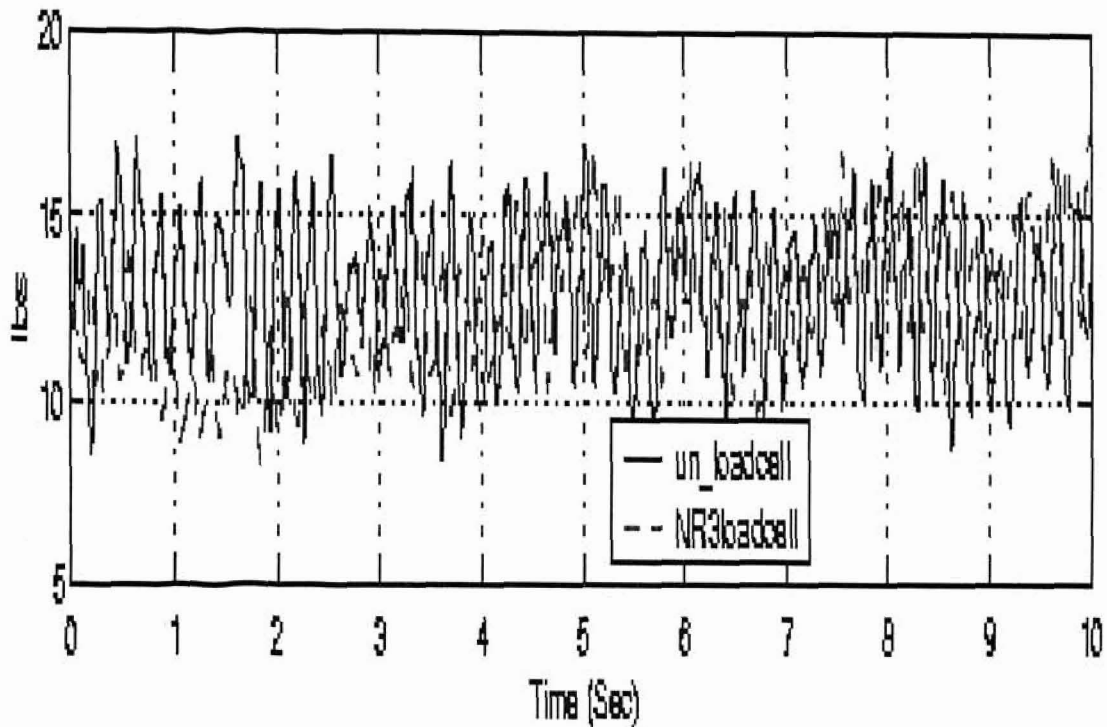


Figure 3.6. Web Line Tension Signals of HSWL

### 3.4 MATERIAL TESTING

The web material properties are essential for the data collected in this research to have value to those attempting to model stresses within 3-D wound rolls. The properties which were tested and determined in this experiment are the radial and in-plane modulus for the webs used and the friction coefficients. Friction coefficients were measured between web layers and between a web layer and an aluminum surface. The friction between the nip roll surface can be important in determining the wound-on-tension (WOT) in the outer layer.

### 3.4.1 Thickness Profile of Webs Across the Web Width

Two different polyester(PET), of nominal thickness of 0.002 and 0.003 inches webs were used in this research. Samples of both types of webs were cut so that web thickness variation could be measured across the width. The 0.002-in thick(2mil) web was 24-in wide and the 3mil thick web was 12-in wide. Webs were cut into ten strips and they were stacked on the top of each other. Forty six measurements, equally spaced were made across the width of 12 inch wide web, and ninety two equally spaced measurements were made across the width of the 24 inch wide web using a digital micrometer which has a resolution of 0.00005-in. The readings were later divided by ten to obtain a single layer thickness. The method was repeated twice and average readings were obtained.

The average widthwise thickness traces obtained for both 2-mil and 3-mil PET webs used are shown in Figures 3.7 . The thickness profile for the 3-mil polyester shows higher thickness at both edge sides and lower thickness on the center of the web. The 2-mil polyester web shows a uniform thickness profile across the width of the roll.

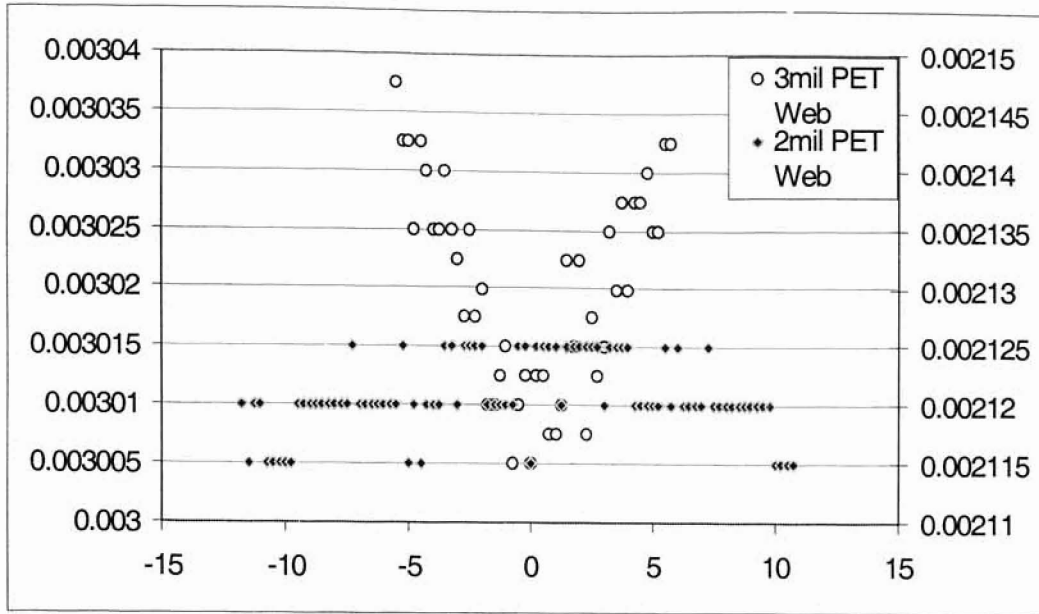


Figure 3.7. Widthwise Thickness Profile of 2mil and 3mil PET Web

### 3.4.2 In-Plane Modulus ( $E_t$ ) Test

The procedure used for testing the in-plane modulus of webs was described by Balaji [8]. Tests were repeated thrice and average values of the modulus were recorded as the in-plane modulus of web. The in-plane moduli of 2-mil and 3-mil PET webs used are given in the table 3.2. An example plot of a stress-strain curve for 3-mil PET web is shown in Figure 3.8.

Web	2-mil PET	3-mil PET
$E_t$ (psi)	550000	737650

Table 3.2. Results of In-Plane Modulus Tests for Various Web Materials

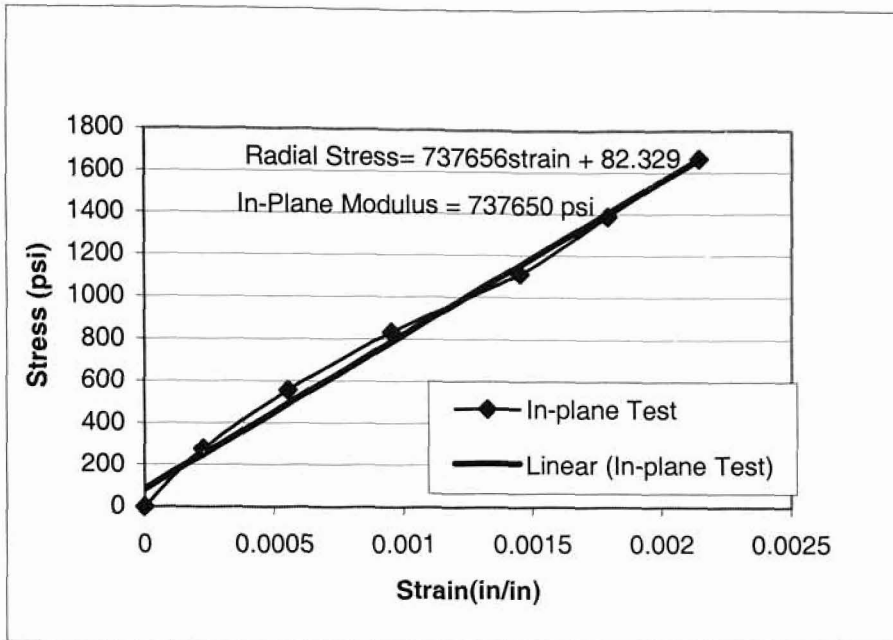


Figure 3.8. Stress-strain Curve for 3-mil PET for In-plane Modulus Test

### 3.4.3 Friction tests:

In this study, friction tests were performed to determine the coefficient of friction between web to web and web to aluminum core. A known weight of 10 lbs was used to measure the friction factors. The weight was fixed to one end of a piece of PET web. The web passed over the aluminum core clamped at both ends. A force gauge was used to pull the web at constant velocity and the pull force was recorded. Three tests were performed and the average pull force was used to determine the coefficient of friction between web and aluminum. The kinetic coefficient of friction was then obtained using the capstan expression:

$$\frac{T_1}{T_2} = e^{\mu_k \theta} \quad \text{Equation (3.8)}$$

where  $\mu_k$  is the kinetic coefficient of friction and  $\theta$ , the angle of wrap was  $\pi$  rads.

Similar tests were performed to determine the coefficient of friction between web layers. The aluminum core was first wrapped with a piece of PET web and the coefficient was measured. The results are summarized in table 3.3.

Coefficient of friction ( $\mu$ )	
$\mu_{\text{Aluminum-2mil PET}}$	0.10
$\mu_{\text{2mil PET-2mil PET}}$	0.18
$\mu_{\text{Aluminum-3mil PET}}$	0.30
$\mu_{\text{3mil PET-3mil PET}}$	0.32

Table 3.3. Coefficient of Friction Factors

#### 3.4.4 Radial Modulus Tests

Pfeiffer [15] created a wound roll model to determine the internal stresses. Pfeiffer found that there was a logarithm relation between pressure and strain in stacks of paper webs.

$$P_c = K_1 \left[ e^{(k_2 \epsilon_c)} - 1 \right] \quad \text{Equation (3.9)}$$



Differentiating yields:

$$E_r = \frac{dP_c}{d\varepsilon_c} = K_2 K_1 \exp(K_2 \varepsilon_c)$$
$$= K_2 [P_c + K_1] \quad \text{Equation (3.10)}$$

where  $\varepsilon_c$  = compressive strain

$P_c$  = compressive pressure

$K_1$  = residual pressure

$K_2$  = constant (Springiness Factor)

The value of  $K_1$  is equal to the pressure on the sheets when the strain is reduced to zero. One would expect this pressure to be zero but there is a slight pressure on a vertical stack, in this case due to the weight of the sheets themselves.

Balaji [8] showed the methods of determining the radial modulus ( $E_r$ ) from the Pfeiffer's expressions as shown in equations 3.9 and 3.10 with a series of pressure-strain data values which were obtained from tests. A LabView program was used for data acquisition and control. A material testing system was used to compress stacks of web material whilst pressure and strain data were recorded. A plot of radial moduli of 2-mil and 3-mil PET webs and pressures is shown in figure 3.9.

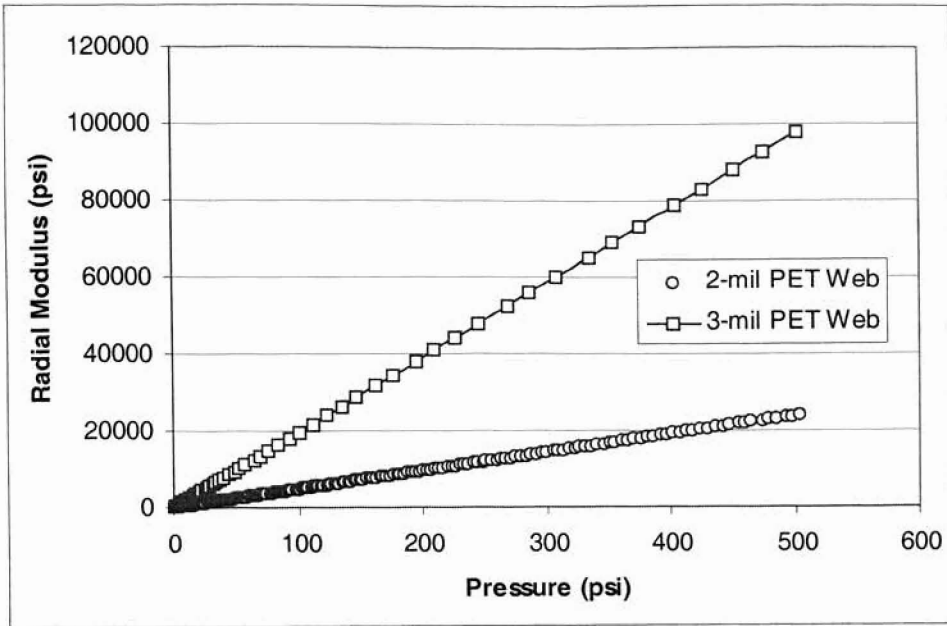


Figure 3.9 Radial Moduli of PET Webs

Web	K1	K2
2-mil PET Web	0.72	47.87
3-mil PET Web	0	194.94

Table 3.4 Coefficients of K1 and K2 in Pfeiffer's Equation

## CHAPTER 4

### EXPERIMENTAL RESULTS AND DISCUSSION

#### 4.1 In-roll Pressure Dependency on Web Widthwise Thickness and Nip Load:

In these experiments, a 24-inch wide web, nominally 0.002 inches thick, and a 12-in wide polyester web, nominally 0.003 inches thick were wound on the instrumented core discussed in chapter 3, at various levels of tension with center winding and various levels of nip loads at center winding with an undriven nip roller. Very low winding speeds of 100 fpm for the rolls were chosen to minimize the effects of air entrainment on in-roll stresses. Rolls were wound at fixed conditions of web tension and nip load. During the winding of each of the rolls, the winder was stopped several times with the web tension maintained in the machine, so that measurements pressure at the core could be performed as a function of CMD location and pile height.

Figure 4.1 shows the repeatability of tests on rolls center wound using 2-mil PET web at 1 pli web tension with a nip load of 3.33 pli. The maximum percentage difference for this experiment is 2.4%. The tension variation in the unwind section that was reported in Figure 3.6 was initially a concern, but these winding repeatability tests have shown this not to be a problem. When center winding with or without a nip roll of the web tension becomes part of the WOT in the outer layer of the winding roll. The good repeatability shown in Figure 4.1 must be a result of either a better tension control in the rewind zone

or because winding is an integral process in which the mean level of web tension has more influence on the roll pressures than the dynamic components of tension.

The pressure profiles versus CMD shown later in this chapter are the average of every trial experiment that was performed. Pile height is defined as the radial depth of web material wound onto the core.

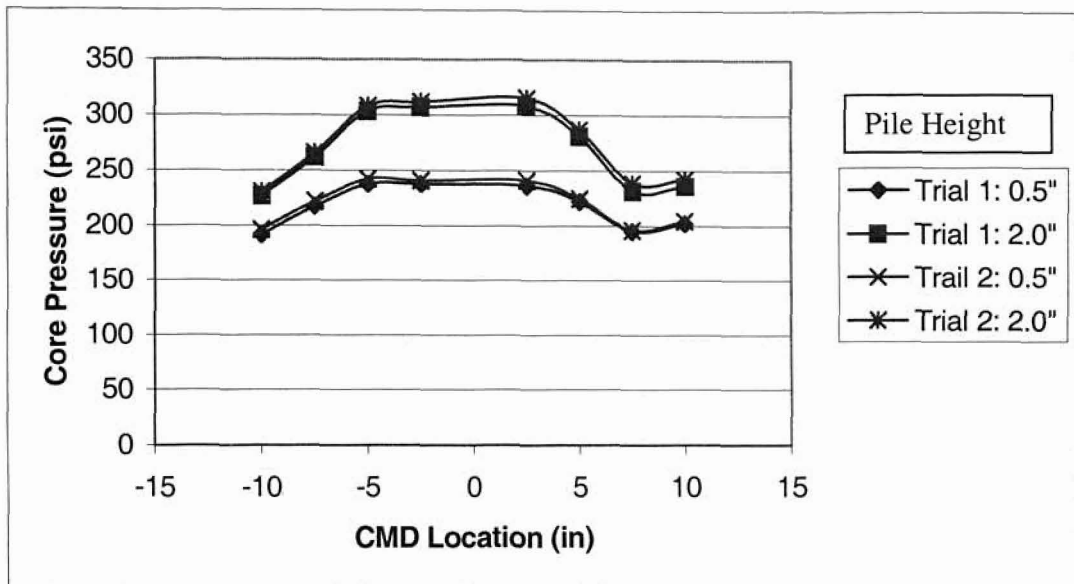


Figure 4.1. Repeatability Tests for Center Wound Rolls With 3.33 pli of Nip Load and 1 pli Web Tension

Figure 4.2 and Figure 4.3 show the core pressure profiles for 2-mil PET web versus the CMD. These rolls were center wound with a constant web line tension of 1 pli and 2 pli respectively. From the results, it is shown that the core pressure has higher values at web tension of 2 pli than 1 pli and appears to vary with the thickness. The core pressures are pretty uniform across the central web width as is the thickness of the web per figure 3.7. The core pressure does decrease near the web edges as the web thickness does as well. Thus it appears there is qualitative agreement between the measured pressure profiles and the thickness profiles in the CMD.

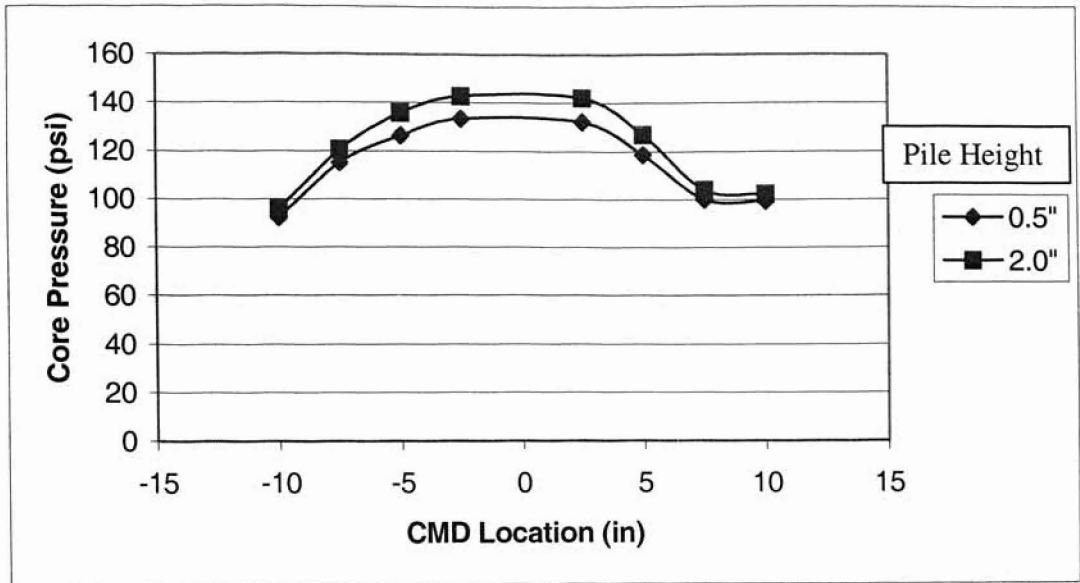


Figure 4.2. Core Pressure Profile For the 2-Mil PET Web Wound at a Web Tension of 1 pli

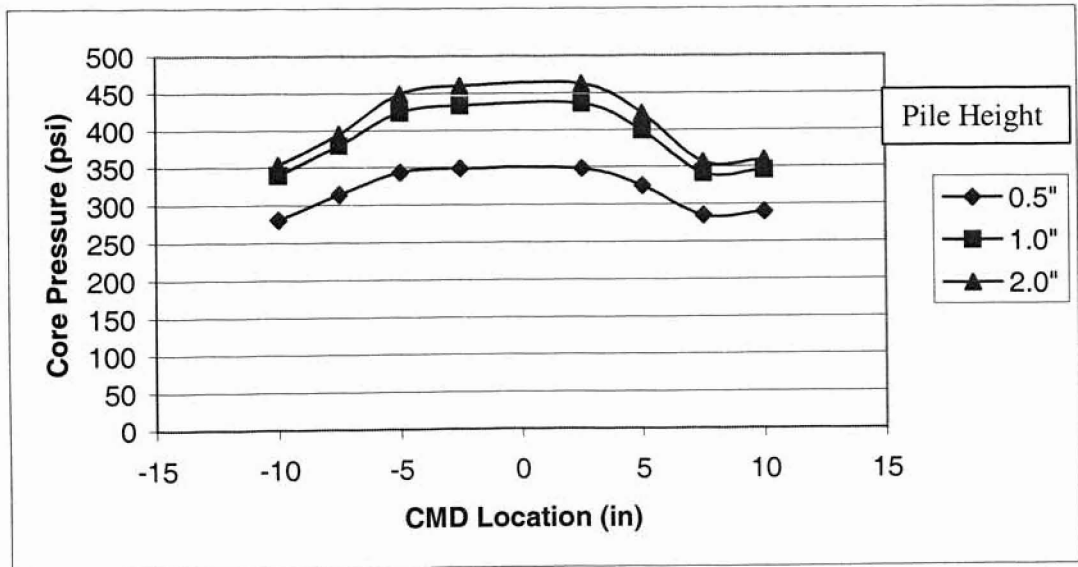


Figure 4.3. Core Pressure Profile For the 2-Mil PET Web Wound at a Web Tension of 2 pli

Past research[1] has shown that the rolls wound with an impinging nip roller produced a harder, higher pressure roll as compared to those wound rolls without any nip. A higher core pressure would be expected as compared to those wound rolls without an impinging nip roller. Shown in figures 4.4 and 4.5, are experiments results of two performed at the same web tension of 1 pli but with a nip load of 3.33 pli and 6.67 pli respectively, on the 2-mil PET web. Figure 4.4 shows higher core pressures as compared to core pressure on figure 4.2 that has been run at the same web tension while center winding but without any nip roller. Figure 4.5 shows a higher core pressure than figure 4.4 due to doubling the nip load. Thus from figures 4.2 through 4.5 it is shown that both increases in web tension and nip load result in increases in core pressure. Although there is variation across the width this follows the trend shown by Expression (2.2). If the pressure beneath the outer layer is affected by web tension and nip load it is reasonable that core pressure should follow the same trend.

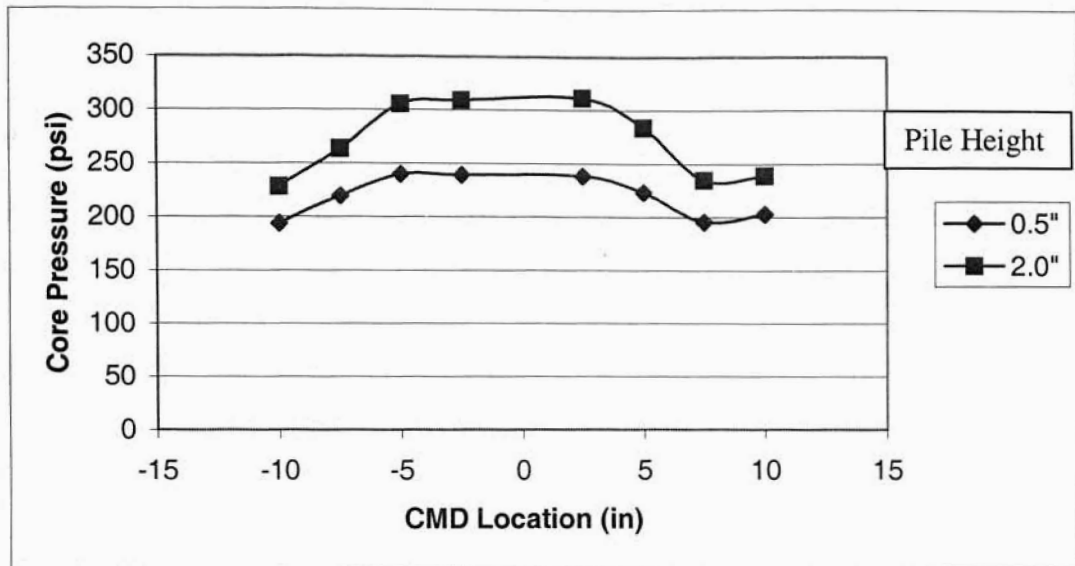


Figure 4.4. Core Pressure Profile For the 2-Mil PET Web Wound at a Web Tension of 1 pli and Nip Load of 3.33 pli

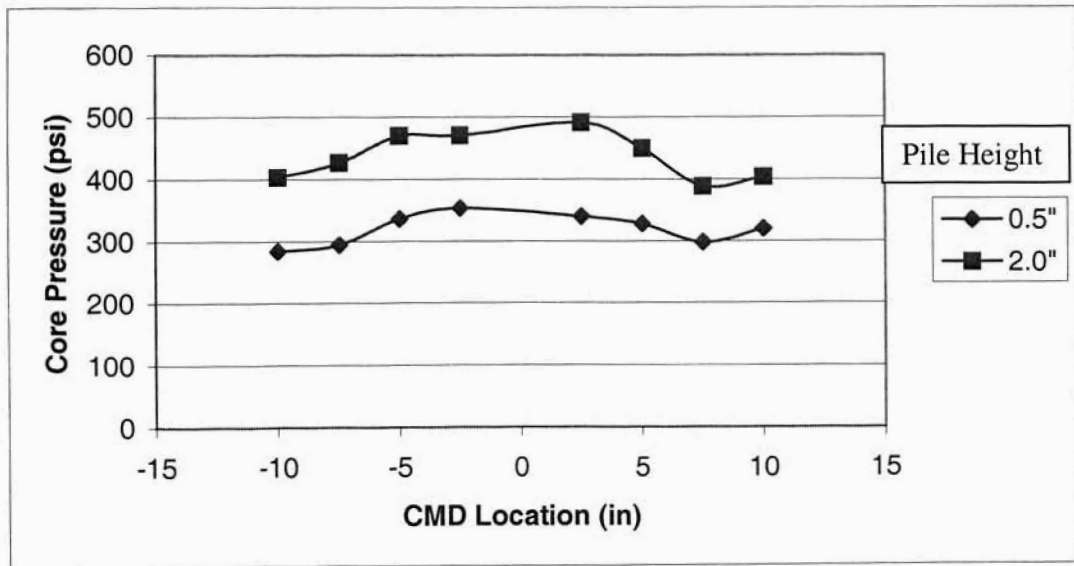


Figure 4.5. Core Pressure Profile For the 2-Mil PET Web Wound at a Web Tension of 1 pli and Nip Load of 6.67 pli

The 3-mil PET web had a large thickness variation and was thinner at the center than at the edges. Figures 4.6 and 4.7 were the experimental results from center winding of polyester web at web line tension of 1 and 2 pli respectively. As from the both figures, the core pressures drop across the CMD. Figure 4.7 shows much higher core pressure as compared to core pressure in figure 4.6.

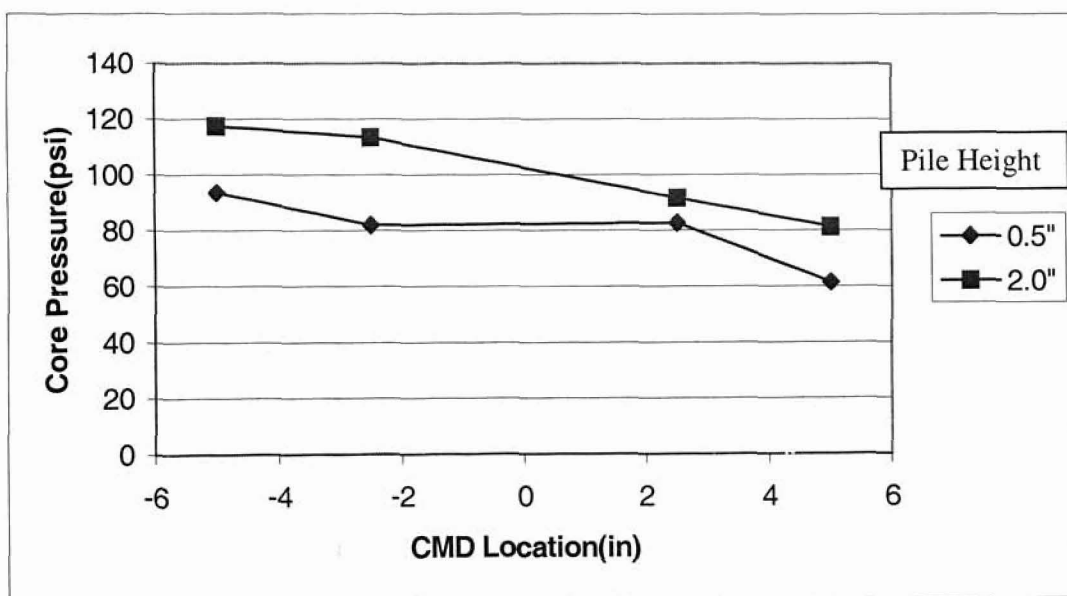


Figure 4.6. Core Pressure Profile For the 3-Mil PET Web Wound at a Web Tension of 1 pli



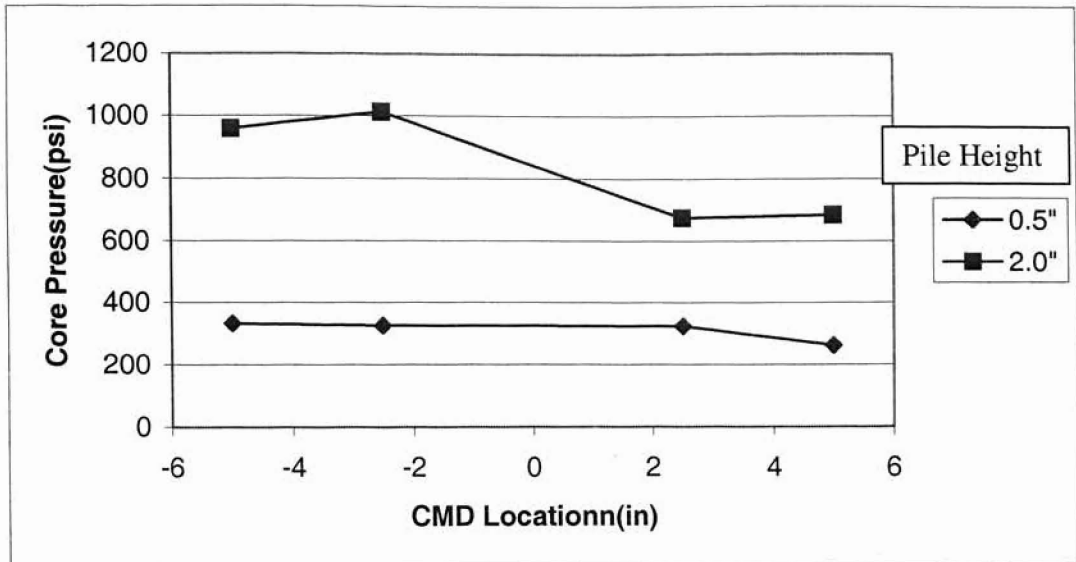


Figure 4.7. Core Pressure Profile For the 3-Mil PET Web Wound at a Web Tension of 2 pli

Air entrainment is suspected in Figures 4.6 and 4.7. Root mean square(RMS),  $R_q$ , and average surface roughness,  $R_a$ , of 3mil PET web were measured by using Multitoyo Profilometer (Model 402). Both surface roughness are shown in Table 4.1.

Surface Roughness of 3mil PET Web ( $\mu$ in)	
$R_q$ : 7	$R_a$ : 5

Table 4.1. Surface Roughness of 3mil PET Web

Air gap of the roll is calculated and is compared to the  $R_q$  of the web. From the result of calculation, air gap,  $h_o$ , shows a greater value than  $3R_q$ .

$$h_o = 0.643R \left( \frac{12\eta V}{T} \right)^{\frac{2}{3}}$$

where  $R$  is the radius of the roll from the core (in)

$\eta$  is the viscosity of air at room temperature ( $\text{lb}_f \text{ s} / \text{ft}$ )

$V$  is the velocity of the web (ft/s)

$T$  is the web tension ( $\text{lb}_f$ )

With a  $12 \text{ lb}_f$  of web tension and a velocity of  $1.67 \text{ ft/s}$  for the experiment, the air gap was found to be 24-micro-inch for a roll radius of 0.5-inch. It is greater than 3 times of  $R_q$ . Therefore, air entrainment occurs during the experiment of center winding for 3mil web.

Next the 3-mil PET web was center wound with an undriven nip roller. Varying nip loads have been applied on the winder core during winding process. Figure 4.8 shows the result of a test which was run at web tension of 1 pli and nip load of 3.33 pli. Figure 4.9 shows the result of tests run at the same web tension as figure 4.8 but with a nip load of 6.67 pli

Figures 4.10 and 4.11 show the tests were run at web tension of 2 pli and 1.5 pli respectively but with different nip loads. The core pressures in figure 4.9 are significantly higher than the web line tension of 1 pli and nip load of 3.33 pli but less than the web line tension of 2 pli and nip load of 3.33 pli. . The additional 1 pli web tension almost doubled the core pressures. Thus, web tension must be affecting the core pressure and the wound-on tension (WOT) more than nip load.

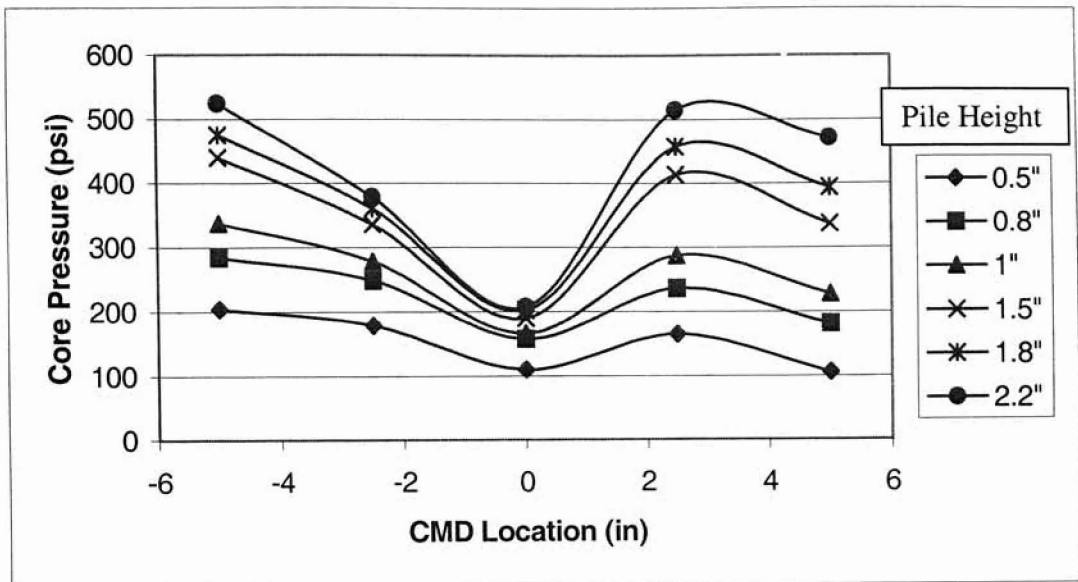


Figure 4.8 . Core Pressure Profile For the 3-Mil PET Web Wound at a Web Tension of 1 pli and Nip Load of 3.33 pli

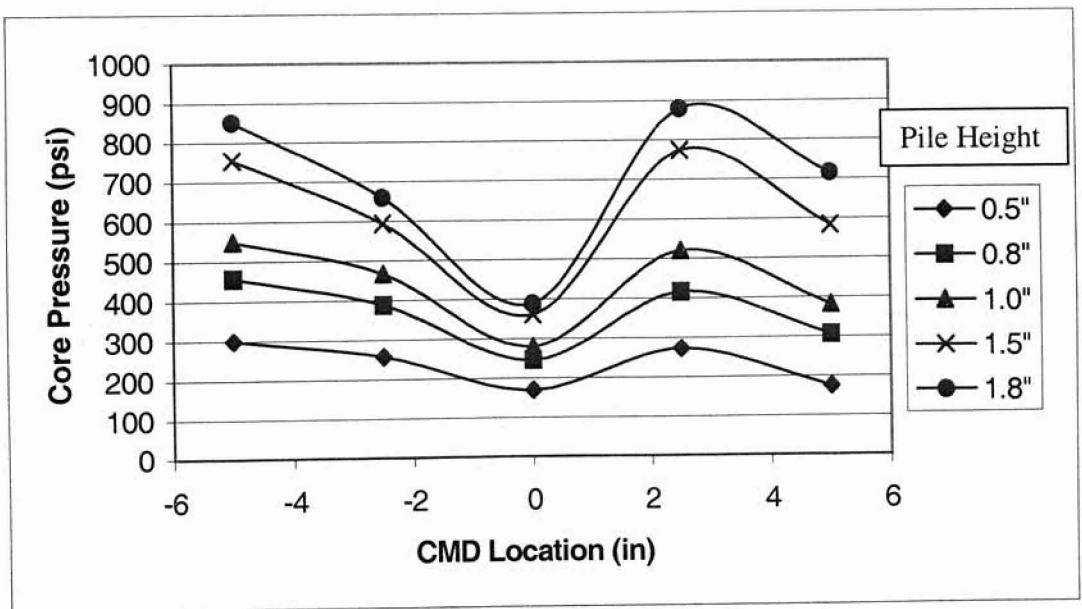


Figure 4.9 . Core Pressure Profile For the 3-Mil PET Web Wound at a Web Tension of 1 pli and Nip Load of 6.67 pli

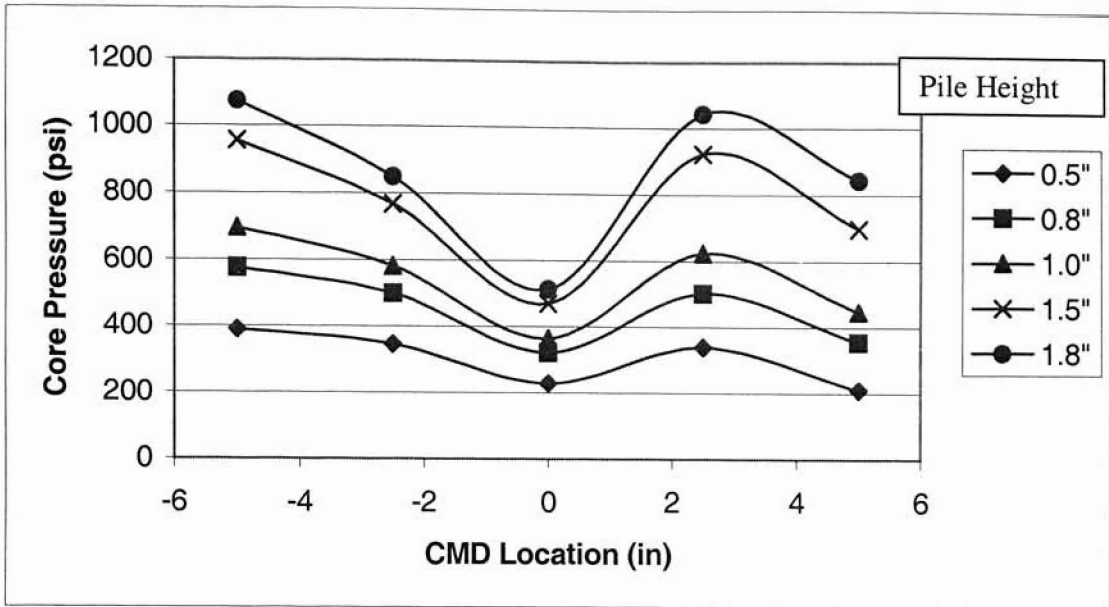


Figure 4.10. Core Pressure Profile For the 3-Mil PET Web Wound at a Web Tension of 2 pli and Nip Load of 3.33 pli

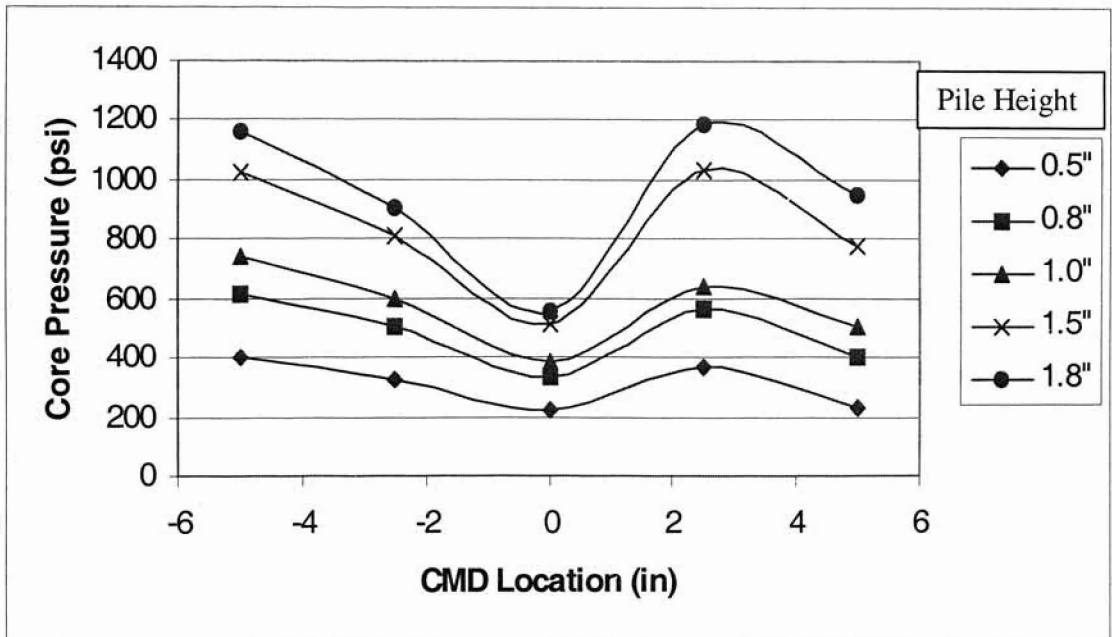


Figure 4.11. Core Pressure Profile For the 3-Mil PET Web Wound at a Web Tension of 1.5 pli and Nip Load of 6.67 pli

## CHAPTER 5

### CONCLUSIONS

The following conclusions are drawn from the experiments carried out which evaluated the roll structure using core pressure measurements.

- 1) Zones of high pressure were found to be dependent on the winding tension level, the number and amplitude of widthwise thickness variations in the web and nip load level.
- 2) Web tension affects WOT more than nip load. (Refer Figures 4.10, 4.11 and 4.12). This is consistent with research reported by Good, Hartwig and Markum [10].
- 3) If a few areas in the widthwise thickness distribution are significantly higher than the rest of the web, high pressure zones will locally develop. If there are many such high spots in the average thickness profile, winding tension becomes distributed over the high spots and none of them cause high zones of pressure in the roll. (Figures 4.10 and 4.6)
- 4) It appears that increases in web tension and nip load serve to increase core pressure at all widthwise locations when the nip roller is engaged. When center winding without a nip the results (Figure 4.4) were consistent with the findings of Hakiel and Cole [6] and Kedl [7]. Their work showed that the WOT was allocated across the web width as a function of a wound roll radius. Those locations with larger outer radii received larger portion of the total WOT than those locations with smaller radii.

## **FUTURE WORK**

The following suggestions are offered as improvement which could be made or are being made to facilitate better roll structure measurements for webs wound from non-uniform webs:

- 1). Web line tension measurement profile across the web width is currently under development on the HSWL.
- 2). Non contact WOT measurement has recently been proven possible this should be developed for the HSWL such that WOT can be profiled across the width of the winding roll.

## References

1. Pfeiffer, J.D., "Mechanics of a Rolling Nip on Paper Webs," TAPPI Journal, Vol.51, No. 8, pp77A-85A, 1968
2. Monk, D.W., Lautner, W.K. and McMullen J.F. " Internal Stresses Within Rolls of Cellophane", TAPPI Journal, Vol. 58, No. 8, pp. 152-155, August 1975
3. Good, J.K., and Fikes, M.W.R., "Predicting the Internal Stresses in Center-Wound Rolls with an Undriven Nip Roller", TAPPI Journal, Vol. 74, No. 6, pp. 101-109, June, 1991
4. Rand, T. and Eriksson, L.G., " Physical Properties of Newsprint Rolls During Winding", TAPPI Journal, Vol. 56, No. 6. Pp.153-156, June,1973
5. Hakiel, Z., "Nonlinear Model for Wound Roll Stresses", TAPPI Journal, Vol. 70, No. 5, pp. 113-117, 1987
6. Cole, K.A. and Hakiel, Z., " A Nonlinear Wound Roll Stress Model Accounting for Widthwise Web Thickness Nonuniformities", Vol. 149, Web Handling, pp. 13-24, ASME 1992
7. Kedl, D.M., " Using a Two Dimensional Winding Model to Predict Wound Roll Stresses that Occur Due To Circumferential Steps in Core Diameter or to Cross-Web Caliper Variation", Proceedings of the First International Conference on Web handling, Oklahoma State University, May 19-22, 1991
8. Balaji, K.K., " A Study of Wound-On Tension Measurement Method in Surface Winding Condition on Tyvek Webs", M.S. Thesis, Oklahoma State University, 2001

9. Good, J.K, Wu, Z., and Fikes, M.W.R., “ The Internal Stresses in Wound Rolls With the Presence of a Nip Roller”, Journal of Applied Mechanics, Vol. 61, pp. 182-185, Mar 1994
10. Good, J.K., Hartwig, J.L., Markum, R., “ A Comparison of Center and Surface Winding Using The Wound In Tension Method”, Proceedings of the Fifth International Conference on Web Handling, WHRC, Oklahoma State University, 2000
11. Shigley, J.E. and Mitchell, L.D., “ Mechanical Engineering Design”, Fourth Edition, pp. 70-73, McGraw-Hill, New York
12. Timoshenko, S., “Theory of Elastic Stability”, First Edition, pp. 445-453, McGraw-Hill, New York
13. Dally, J.W., “ Experimental Stress Analysis”, pp.74-77, McGraw-Hill, New York
14. Pagilla P.R. and Shelton J.J., “ Dynamics of Motor, Controller and Mechanical Drive for Tension Control”, Web Handling Research Center Semiannual Technical Review and Industry Advisory Board Meeting, June 2002.
15. Pfeiffer, J.D., “ Internal Pressures in a Wound Roll of Paper”, TAPPI Journal, Vol.51, No. 8, pp. 342-347, Aug 1968



## APPENDIX A

- 1. IN-PLANE MODULUS OF 2-MIL PET WEB**
- 2. PHOTOGRAPHS OF HIGH SPEED WEB LINE**
- 3. NUMERICAL CORE PRESSURE DATA FROM ALL WINDING  
EXPERIMENTS ON 2 AND 3 MIL PET WEBS**

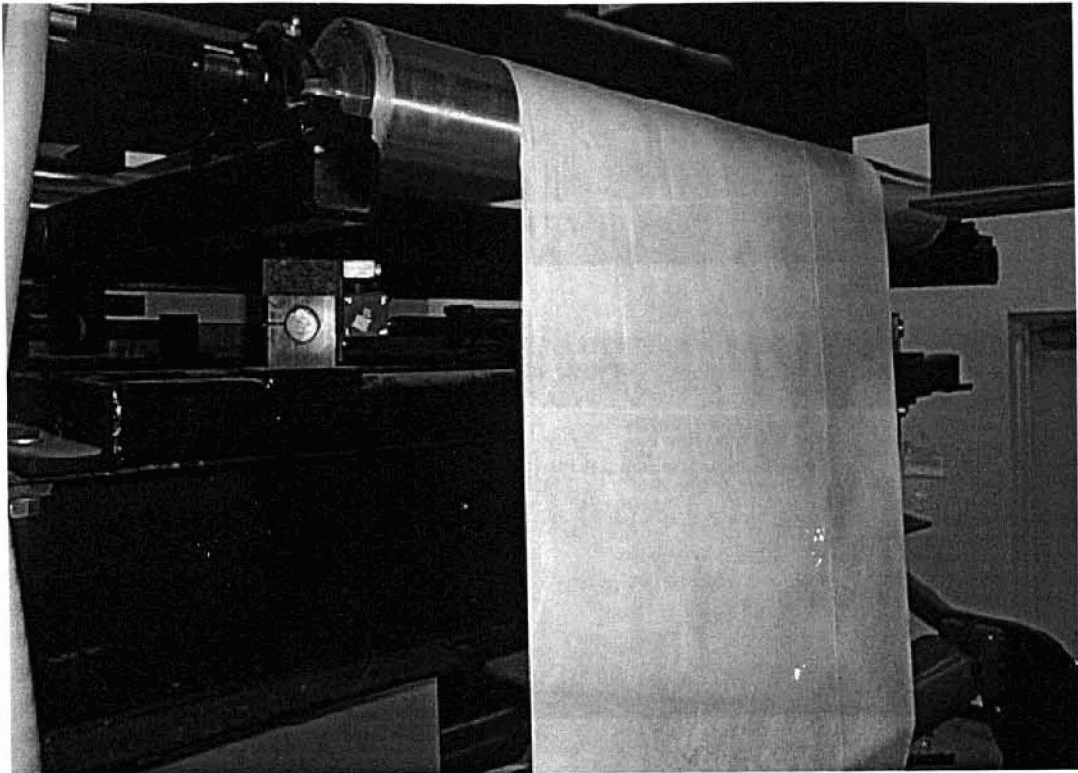


Figure A-1: Web Guide of HSWL

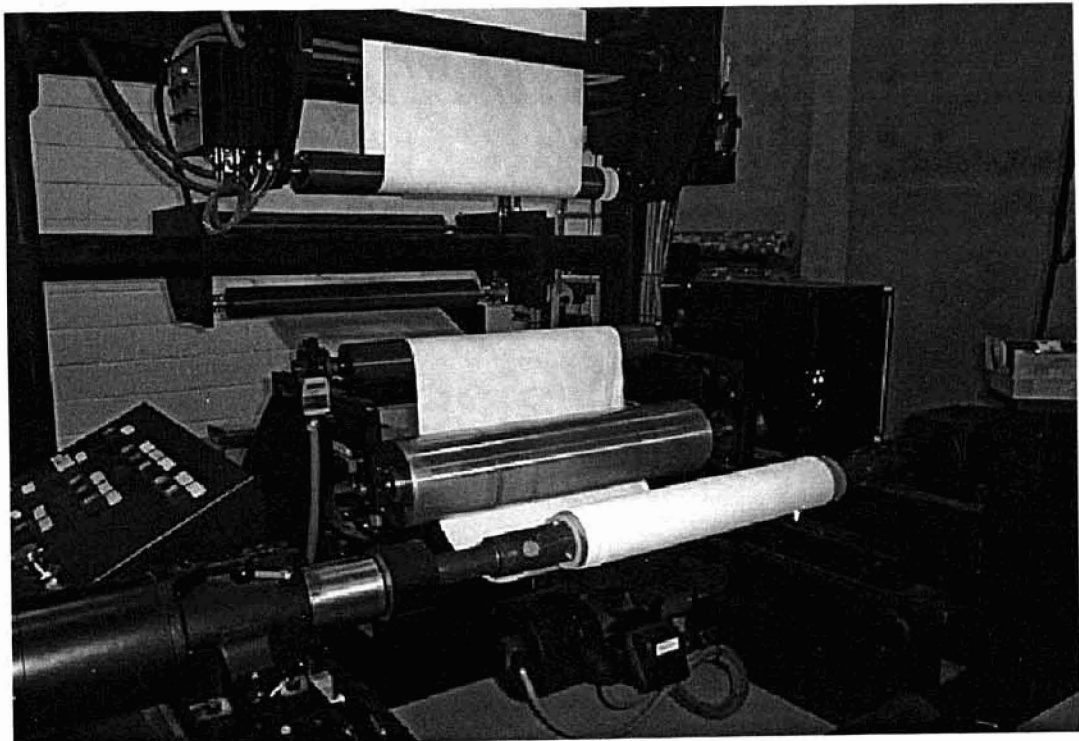


Figure A-2: Rewind Station of HSWL

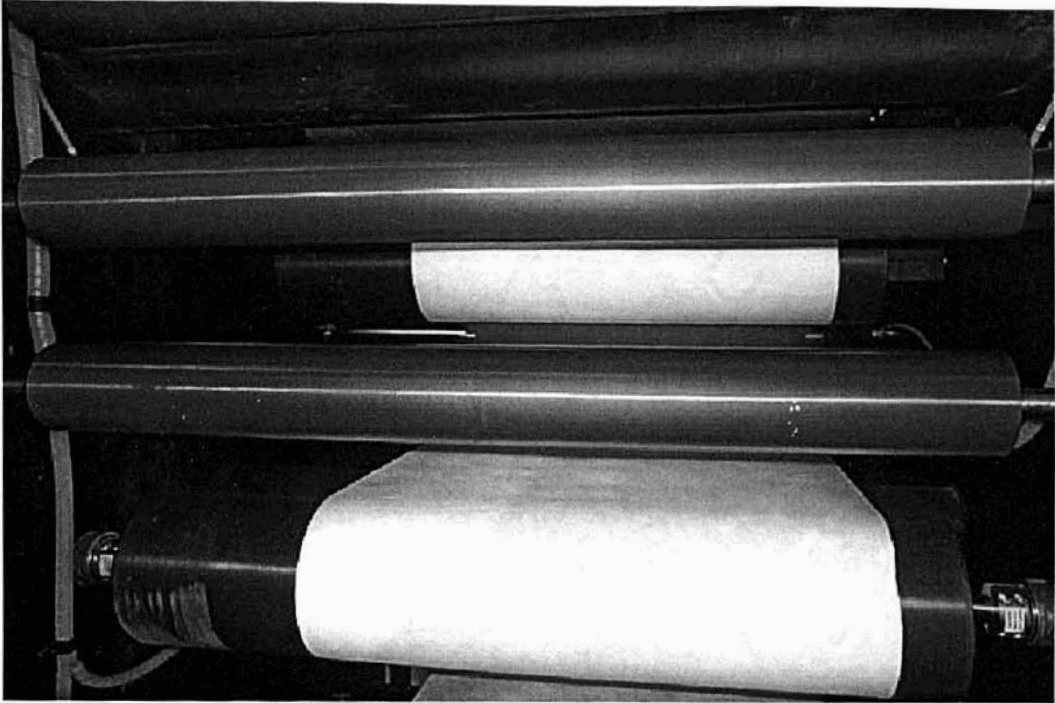


Figure A-3: Nip Station 1 of HSWL

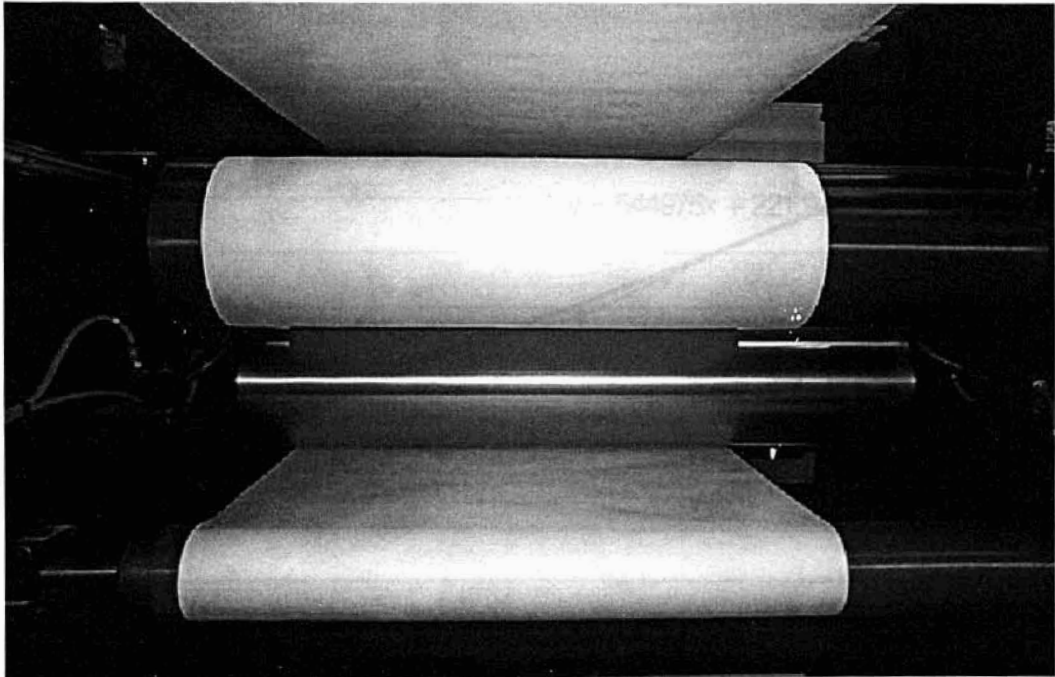


Figure A-4: Nip Station 2 of HSWL

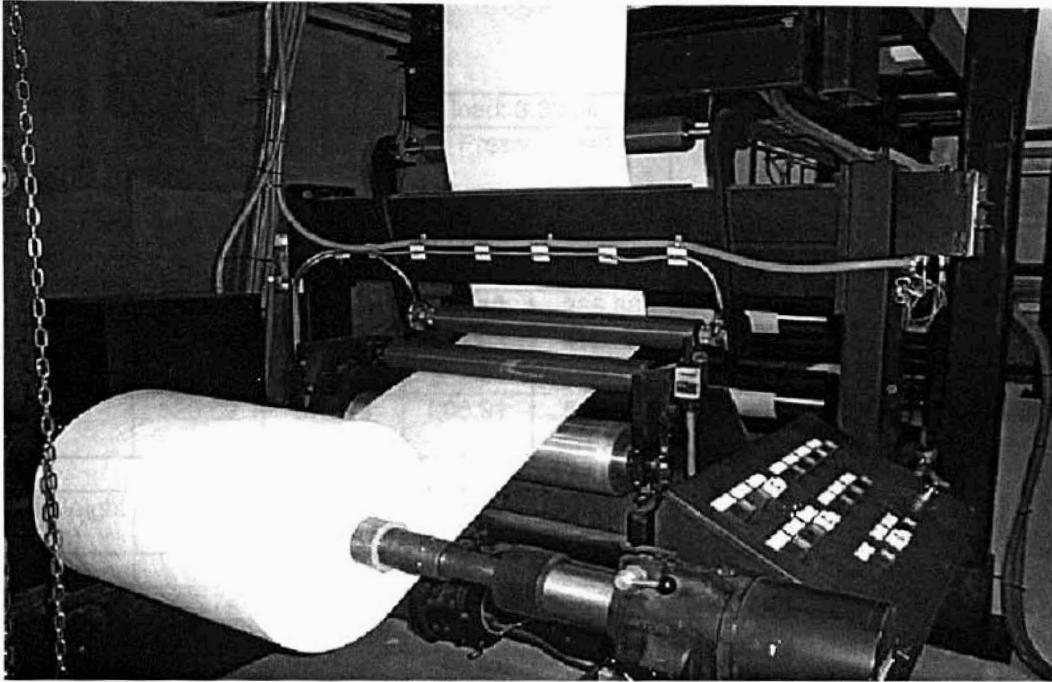


Figure A-5: Unwind Station of HSWL

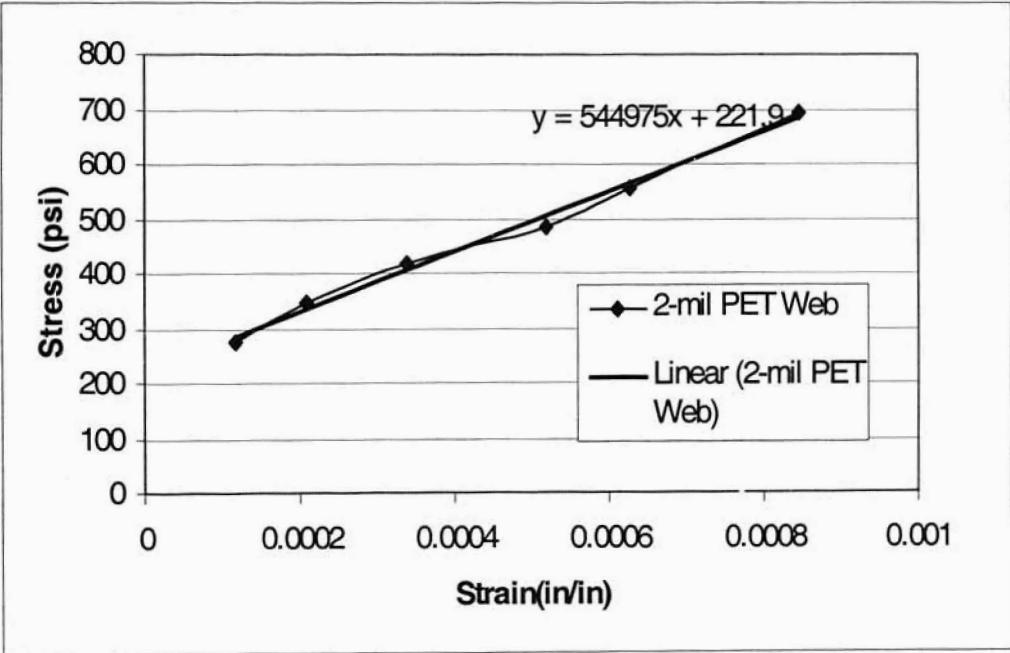


Figure A-6: Stress-strain Curve for 2-mil PET for In-plane Modulus Test

Table A-1: Numerical Core Pressure Data for 3-mil PET Web

3-mil PET Web

Web line tension: 1pli		Nip load: 3.33 pli			
Pile Height (in)	Pressure(psi)				
	-5	-2.5	0	2.5	5
0.5	203.38	179.87	111.67	163.41	106.98
0.8	286.86	250.41	152.83	233.95	184.57
1	338.58	279.80	168.12	286.86	229.46
1.5	442.04	336.23	191.63	412.66	336.23
1.8	480.85	362.10	202.21	456.15	397.37
2.2	526.69	379.74	206.91	516.11	470.26

Pile Height (in)	Pressure(psi)				
	-5	-2.5	0	2.5	5
0.5	205.74	178.7	109.34	166.95	105.81
0.8	282.16	248.07	162.24	239.84	179.88
1	336.24	277.46	164.59	289.22	226.91
1.5	440.88	336.24	189.28	415.01	338.59
1.8	470.27	360.93	203.39	459.69	391.5
2.2	523.18	378.57	208.09	513.77	472.62

Web line tension: 2pli		Nip load: 3.33 pli			
Pile Height (in)	Pressure(psi)				
	-5	-2.5	0	2.5	5
0.5	386.8	342.12	224.55	338.59	208.09
0.8	577.26	499.66	319.78	504.36	357.41
1	698.35	584.31	364.46	628.99	451.46
1.5	955.82	766.54	467.92	925.26	699.53
1.8	1072.2	847.66	511.42	1044	844.13
Pile Height (in)	Pressure(psi)				
	-5	-2.5	0	2.5	5
0.5	396.2	351.53	233.96	343.3	215.15
0.8	576.08	500.84	325.66	500.84	356.23
1	692.47	581.96	367.99	619.58	446.76
1.5	958.18	768.89	472.62	921.73	696
1.8	1078.1	851.19	514.95	1041.6	844.13

Web line tension: 1 pli		Nip load: 6.67 pli			
Pile Height (in)	Pressure(psi)				
	-5	-2.5	0	2.5	5
0.5	295.09	265.7	172.82	266.88	174
0.8	452.64	398.55	245.72	413.84	306.85
1	546.69	466.74	280.99	522	386.8
1.5	748.91	600.77	358.58	771.24	585.49
1.8	845.31	666.61	387.97	878.23	720.69

Pile Height (in)	Pressure(psi)				
	-5	-2.5	0	2.5	5
0.5	305.68	249.24	166.95	279.81	177.53
0.8	460.86	378.57	245.72	418.54	305.68
1	552.57	466.74	279.81	519.65	379.74
1.5	760.66	587.84	364.46	777.12	581.96
1.8	857.07	652.5	390.32	882.93	711.28

Web line tension: 1.5 pli		Nip load: 6.67 pli			
Pile Height (in)	Pressure(psi)				
	-5	-2.5	0	2.5	5
0.5	403.26	331.54	229.26	371.51	233.96
0.8	612.53	507.89	335.07	565.5	402.08
1	732.45	594.89	379.74	577.26	498.49
1.5	1022.8	817.09	507.89	1038.1	775.95
1.8	1163.9	908.8	547.86	1185.1	951.12

Pile Height (in)	Pressure(psi)				
	-5	-2.5	0	2.5	5
0.5	395.03	313.91	219.85	356.23	223.38
0.8	614.88	502.01	330.36	560.8	400.91
1	746.55	599.59	391.5	703.05	505.54
1.5	1021.7	798.28	509.07	1032.2	770.07
1.8	1163.9	900.57	560.8	1181.6	944.07

center winding: 1 pli		pressure(psi)		
Pile Height (in)				
	-5	-2.5	2.5	5
0.5	91.6	73.83	82.03	61.52
2	116.22	113.48	90.23	80.66
0.5	95.70	90.23	83.4	61.52
2	118.94	113.48	92.96	82.03

center winding: Tw 2 pli		pressure(psi)		
Pile Height (in)				
	-5	-2.5	2.5	5
0.5	332.25	325.4	322.66	259.77
2	976.22	998.09	659.02	663.12
0.5	334.97	328.14	325.4	265.25
2	944.77	1030.9	693.2	706.88

Table A-2: Numerical Core Pressure Data for 2-mil PET Web

2-mil PET Web: Web Tension of 1 pli								
	pressure(psi)							
Pile Height(in)	-10	-7.5	-5	-2.5	2.5	5	7.5	10
0.5	94.05	117.57	127	132.85	132.85	118.74	99.93	99.93
2	95.23	119.92	132.9	142.26	141.08	125.8	103.46	102.28
0.5	90.52	112.86	125.8	134.03	131.68	118.74	99.93	98.75
2	96.40	121.09	138.7	143.43	143.43	128.15	104.64	102.28

2-mil PET Web: Web Tension of 2 pli								
	Pressure(psi)							
Pile Height (in)	-10	-7.5	-5	-2.5	2.5	5	7.5	10
0.5	279.81	312.73	339.8	345.65	344.47	323.31	284.51	289.22
1	337.42	376.22	424.4	433.82	436.18	399.73	341.53	345.65
2	350.35	391.5	449.1	460.28	462.63	422.65	356.82	359.76
0.5	282.16	315.08	346.8	351.53	351.53	325.66	285.69	290.39
1	342.12	383.27	429.1	438.53	440.88	404.43	344.47	348
2	356.23	398.55	455	465.57	467.92	426.77	358.58	362.11

2-mil PET Web: Web Tension of 1 pli and Nip Load of 3.33 pli								
	pressure(psi)							
Pile Height (in)	-10	-7.5	-5	-2.5	2.5	5	7.5	10
0.5	191.63	217.49	237.5	237.49	236.31	222.2	195.17	202.22
2	226.91	262.17	303.3	306.85	308.03	280.98	231.62	236.31
0.5	196.34	222.2	242.2	241.02	241.02	224.55	196.34	204.57
2	230.43	265.71	308	311.55	315.08	286.86	238.66	242.18

2-mil PET Web: Web Tension of 1 pli and Nip Load of 6.67 pli								
	pressure (psi)							
Pile Height (in)	-10	-7.5	-5	-2.5	2.5	5	7.5	10
0.5	288.05	298.62	339.8	355.06	342.12	330.37	303.32	323.31
2	405.62	431.48	471.4	471.45	494.95	453.82	391.49	407.95
0.5	280.98	291.57	332.7	352.71	338.6	325.66	292.74	317.43
2	400.91	422.06	469.1	470.28	487.91	446.75	385.62	399.72



VITA 2

Eng Sheng Ngoi

Candidate of the Degree of

Master of Science

**Thesis:** EFFECT OF WIDTHWISE WEB THICKNESS NONUNIFORMITIES ON WOUND ROLL STRESSES

**Major Field:** Mechanical Engineering

**Biographical:**

**Personal Data:** Born in Changkat Kruing, Perak , Malaysia, On September 17, 1976, the son of Kuang Phing Ngoi and Siew Ling Ooi

**Education:** Graduated from S.M.J.K. Ayer Tawar Secondary School, Malaysia in December 1994; received Bachelor of Science in Mechanical Engineering from Oklahoma State University, Stillwater, Oklahoma in August 1999. Completed the requirements for the Master of Science degree with a major in Mechanical Engineering at Oklahoma State University, Stillwater, Oklahoma in December 2002.

**Experience:** Employed by the Department of Mechanical Engineering at Oklahoma State University as a graduate assistant, January 2001 to present.